Universidade do Minho
Escola de Ciências

Pedro Rafael Magalhães Veloso

Formulation of a drug delivery platform for the release of 5-aminosalicylic acid in the gastrointestinal tract

Formulation of a drug delivery platform for the release of 5-aminosalicylic acid in the gastrointestinal tract

Pedro Veloso

UMinho | 2021

março de 2021

ColOsH

funbioplas

FCT Fundação para a Ciência e a Tecnologia

REPÚBLICA PORTUGUESA

UNIÃO EUROPEIA
Fundo Social Europeu

Universidade do Minho
Escola de Ciências

Pedro Rafael Magalhães Veloso

Formulation of a drug delivery platform for the release of 5-aminosalicylic acid in the gastrointestinal tract

Dissertação de Mestrado
Mestrado em Biofísica e Bionanossistemas

Trabalho efetuado sob a orientação do(a)
Doutor Raul Machado
Doutora Clarisse Nobre

março de 2021

Acknowledgments

After a very atypical and hard year, I am extremely proud to cross such an important step in my academic journey. I have learned a great deal during these two years and have grown both as a person and as a scientist. While hard work and perseverance play a very important role, I couldn't have succeeded without the help of many people around me whom I can't thank enough.

To my supervisors, Doctors Raul Machado and Clarisse Nobre, who led me on the right path, taught me everything they could and never refused to help me. To all my teachers, for sparking my curiosity for the incredible world of biophysics and nanotechnology. To the lab mates of LBM II, always ready to help, for making my stay feel comfortable and, particularly, to Diana for being so helpful and supportive. To my mother and my father, for always believing I could do great things and always doing everything they could to guarantee my future. To my sister, for always pushing me to strive for greatness and to be the best I could. To Inês, my pillar, my shelter, for being by my side, motivating me whenever I needed it the most and being the best partner I could ever wish for. To all my friends and colleagues, for going through this journey with me and reminding me that work isn't everything in life.

To all of you, words cannot express how much I am thankful for these years and the more to come.

Este trabalho foi financiado por fundos nacionais através da FCT – Fundação para a Ciência e a Tecnologia, I.P., no âmbito do projeto "*FunBioPlas - Novel synthetic biocomposites for biomedical devices*" com referência ERA-IB-2-6/0004/2014 e do projeto "*ColOsH - Novel concept for a dynamic modular Colon system including peristalsis simulation by Oscillatory-flow and Colon-Host interaction*" com referência PTDC/BTM-SAL/30071/2017 (POCI–01–0145–FEDER–030071).

STATEMENT OF INTEGRITY

I hereby declare having conducted this academic work with integrity. I confirm that I have not used plagiarism or any form of undue use of information or falsification of results along the process leading to its elaboration.

I further declare that I have fully acknowledged the Code of Ethical Conduct of the University of Minho.

Formulação de uma plataforma de entrega de fármacos para a libertação de ácido 5-aminossalicílico no trato gastrointestinal

Resumo

Com o aumento da incidência de doenças inflamatórias intestinais (DII), a necessidade de desenvolver e administrar novas terapias é cada vez maior. O ácido 5-aminosalicílico (5-ASA) é um anti-inflamatório não esteroide frequentemente prescrito a pacientes com doença inflamatória intestinal leve, devido à sua segurança e eficácia em certos estados da doença. No entanto, apresenta algumas limitações em estados mais agravados da doença e, em particular, em doença de Crohn, o que realça a necessidade de desenvolver novos sistemas de entrega que melhorarem o seu perfil farmacocinético.

Este trabalho tem como objetivo avaliar o uso de recombinâmeros tipo-elastina (elastin-like recombinamers, ELR) para a formulação de sistemas de entrega de fármacos, focando especificamente no encapsulamento e libertação de 5-ASA para aplicação em terapias de DII. Os ERL são polímeros proteicos produzidos por engenharia genética, inspirados na tropoelastina de mamíferos, que têm sido amplamente estudados para aplicações biomédicas. Uma característica notável dos ELR é a sua transição de fase dependente da temperatura. Quando sujeitos a um estímulo térmico, estes polímeros proteicos auto-organizam-se, formando aglomerados proteicos, num processo completamente reversível. Neste trabalho, o polímero proteico A200 – um ELR composto por múltiplas repetições do pentâmero VPAVG – foi avaliado relativamente à capacidade de encapsular e libertar 5-ASA. Devido ao seu comportamento de transição de fase reversível, a purificação de A200 foi conseguida com recurso a ciclos de aquecimento/arrefecimento, evitando assim a utilização de processos cromatográficos complexos. Este comportamento termorresponsivo foi explorado para o encapsulamento de 5-ASA em condições não agressivas nomeadamente, em PBS e 37 °C. A eficiência do sistema de A200 foi avaliada através da determinação da capacidade de encapsulamento (expressa em termos de quantidade de fármaco encapsulado e capacidade de carga) e cinética de libertação do fármaco, usando espetroscopia de absorção e fluorescência para a quantificação de 5-ASA. A cinética de libertação cumulativa foi avaliada por ajuste dos dados experimentais a uma série de diferentes modelos cinéticos, sugerindo um mecanismo de difusão. Este trabalho contribui para o aumento do conhecimento sobre o potencial de ELR como plataformas de entrega de fármacos, focando no encapsulamento e libertação de moléculas bioativas.

Palavras-chave: Ácido 5-aminosalicílico, doenças inflamatórias intestinais, entrega de fármacos, recombinâmeros tipo elastina

Formulation of a drug delivery platform for the release of 5-aminosalicylic acid in the gastrointestinal tract

Abstract

As the incidence of inflammatory bowel disease (IBD) increases, the need to design and administer new therapies also increase. 5-aminosalicylic acid (5-ASA), a nonsteroidal anti-inflammatory drug, is commonly prescribed to inflammatory bowel disease patients with mild disease due to its safety and effectiveness in earlier disease stages. However, it presents some limitations in advanced disease stages, particularly in Crohn's disease, which highlights the need to develop new delivery systems to improve its pharmacokinetic profile.

The present work aims at assessing the use of elastin-like recombinamers (ELR) as a new drug delivery system, targeting the encapsulation and release of 5-ASAto apply in IBD therapy. ELR are genetically engineered protein polymers, inspired in the mammalian tropoelastin that have been widely studied for biomedical applications. A remarkable feature of ELR is the temperature-dependent phase transition behaviour. Upon a thermal stimulus, the protein molecules self-assemble into protein aggregates, in a fully reversible process. In this work, A200 – an ELR comprising multiple repetitions of the pentamer VPAVG – was evaluated for its ability to encapsulate and release 5-ASA. Due to the reversible phase transition behaviour, the recombinant A200 was easily purified by hot and cold cycles, avoiding the use of cumbersome chromatographic processes. This thermoresponsive behaviour was also exploited for the encapsulation of 5-ASA using mild conditions (PBS and 37 °C). The efficiency of the A200-based system as a drug carrier was assessed by determination of drug loading (expressed as loading capacity and encapsulation efficiency) and release kinetics, using absorbance and fluorescence spectroscopy for 5-ASA quantification. The cumulative release kinetics were evaluated by fitting the experimental data against a series of different release kinetic models. Results provide indications for the physical mechanistic processes behind drug release, indicating that it is dependent on diffusion and polymer swelling. This work contributed to expand the knowledge on ELR as drug delivery platforms, targeted to the encapsulation and release of bioactive molecules.

Keywords: 5-aminosalicylic acid, drug delivery, elastin-like recombinamers, inflammatory bowel disease

Table of Contents

List of Abbreviations

5-ASA – 5-aminosalicylic acid

A – L-Alanine

AdR^2 – Adjusted R^2

AIC – Akaike information criterion

ATR-FTIR – Attenuated total reflectance Fourier transform infrared spectroscopy

BMPs – Bone morphogenetic proteins

CD – Crohn's disease

COX – Cyclooxygenase

CRC – Colorectal cancer

CS – Cooling stage

DLS – Dynamic light scattering

DMP – Dexamethasone phosphate

DSC – Differential scanning calorimetry

EE – Encapsulation efficiency

ELP – Elastin-like polypeptides

ELR – Elastin-like recombinamers

ELS – Electrophoretic light scattering

G – Glycine

GIT – Gastrointestinal tract

HPA – Hypothalamic-pituitary-adrenal

HPLC – High performance liquid chromatography

HS – Heating stage

IBD – Inflammatory bowel disease

IFN-γ – Interferon gamma

IL – Interleukin(s)

ITC – Inverse transition cycling

ITT – Inverse temperature transition

IUPAC – International Union of Pure and Applied Chemistry

K – L-Lysine

Kan - kanamycin

LB – Lysogeny broth

LC – Loading capacity

MMX® – Multi matrix

MSC – Model selection criterion

MWM – Molecular weight marker

NAT – N-acetyl transferase

NF-κB – Nuclear Factor-Kappa B

NSAID – Nonsteroidal anti-inflammatory drug

OD – Optical density

P – Proline

PBS – Phosphate-buffered saline

PCL – Poly(ε-caprolactone)

PDI – Polydispersity index

PLA – Poly(lactic acid)

PLGA – Poly(lactic-co-glycolic acid)

PPARγ – Peroxisome proliferator-activated receptors γ

RI – Refractive index

SCFAs – Short-chain fatty acids

SD – Standard deviation

SDS-PAGE – Sodium dodecyl sulphate polyacrylamide gel electrophoresis

SEM – Scanning electron microscopy

TB – Terrific broth

TBlac – Terrific broth supplemented with 2 g/L of lactose

TE – Tris-EDTA

TNF-α – Tumour necrosis factor-alpha

Ts – Dissolution temperature

Tt – Transition temperature

UC – Ulcerative colitis

V – Valine

ZP – Zeta potential

List of Figures

List of tables

1. Introduction

1.1. Inflammatory bowel disease

Inflammatory bowel disease (IBD) is the general term for a condition that causes inflammation across the gastrointestinal tract (GIT). Its two main forms include Crohn's disease (CD) and ulcerative colitis (UC), both being characterized by chronic recurrent bowel inflammation. CD is characterized by inflammation in any part of the GIT in non-continuous segments and commonly causes abscesses, fistulas and strictures. On the other hand, UC is associated with a general mucosal inflammation and is limited to the colon [1]. IBD is a condition that affects the worldwide population, with increasing incidence over the past years [2,3]. In newly industrialized countries of Africa, Asia and South America, a rising level of incidence has been reported. Still, the highest prevalence of IBD is reported in European countries – 505 per 100 000 person-years for UC in Norway and 322 per 100 000 person-years for CD in Germany – and in North America – 286 per 100 000 person-years in the USA and 319 per 100 000 person-years in Canada [4]. Although no direct cause is established, it is well accepted that the IBD pathogenesis is the result of an excessive and dysregulated immune response to the intestinal microbiota, with genetic and environmental factors playing a major role in the development of the disease [1,5–7].

IBD is not a particularly dangerous disease mortality-wise. However, patients suffering from IBD have a higher risk of developing colorectal cancer (CRC), other gastrointestinal diseases, infections and respiratory diseases, which leads to a slightly higher mortality rate compared to the general population [8–10]. The main concern with this disease is related with its substantial morbidity because symptoms persist throughout life with social, psychological and physical implications [11]. Most patients report urgency of bowel movements and/or losing control over them, abdominal pain and/or cramps and fatigue, among various other symptoms [12]. It is also known that IBD causes extraintestinal manifestations in some patients which include anaemia, nutritional deficiencies, arthritis and lesions [13]. One aspect often overlooked is the mental health impact of the disease. IBD patients show a higher percentage of anxiety and depressive symptoms compared to the general population and the management of these symptoms may play an important role in the disease's treatment [14,15].

There is no known cure for IBD and, therefore, current therapies attempt to mitigate symptoms, stop the disease's progression and overall improve quality of life. Approximately 20 % to 30 % of UC patients and about half of CD patients require surgery in order to remove obstruction, mass or abscess within 10 years of diagnosis [13]. Therefore, pharmaceutical treatments have been employed to delay or prevent surgery,

ideally not increasing the risk of other serious conditions. Being an autoimmune disease, the therapeutic approach is to repress the excessive immune response by immunosuppressive and anti-inflammatory drugs which can have various potential negative effects. The excessive immune response in IBD patients is due to an antigen-specific activation of various lymphocytes present in the intestinal mucosa, induced by microorganisms present in the gut microbiota. This results in an increase in proinflammatory cytokines such as tumour necrosis factor alpha (TNF-α), interferon gamma (IFN-γ) and interleukins (IL) and ultimately inflammatory damage in the gut [16]. There are three main types of drugs presently used in IBD pharmaceutical treatment: corticosteroids, biologics/immunosuppressants and aminosalicylates (**table 1**).

Table 1 - Mode of action and potential side effects of common IBD therapeutic drugs.

Therapy	Mode of action	Potential side effects	Reference
Aminosalicylates	PPARγ-like inhibition of proinflammatory prostaglandins, leukotrienes and cytokines.	Rash, diarrhoea, headache, fever, abdominal pain, impaired renal function, dyspepsia, oedema, dizziness, constipation, arthalgia	17
Corticosteroids	Transcription inhibition of genes in the production of proinflammatory cytokines	Hyperglycaemia, electrolyte imbalance, fluid retention, hyperlipidaemia, hepatic steatosis, emotional disturbances, psychosis, pseudotumour cerebri, glaucoma, cataracts, acne, impaired wound healing, skin atrophy, dyspepsia, osteonecrosis, osteoporosis, myopathy, hypertension, increased infection risk, hypothalamic-pituitary-adrenal (HPA) axis suppression, growth retardation in children	18
Biologics/ immunosupressants	Monoclonal antibodies that bind to TNF-α, integrins or interleukins, stopping proinflammatory cascades	Leucopoenia, thrombocytopenia, anaemia, psoriasis, psoriasiform lesions, erythema nodosum, cardia failure, second and third-degree heart block, arrythmias, demyelination, increased infection risk, melanoma, nonmelanoma skin cancer, lymphoma, leukoencephalopathy	19

Corticosteroids tend to be used in patients with moderate to severe disease. These drugs bind to glucocorticoid receptors and inhibit the transcription of genes involved in the production of inflammatory cytokines such as IL-1, IL-6 and TNF-α, while also inhibiting protein synthesis by affecting the stability of mRNA [20]. Corticosteroids are effective in inducing remission in both UC and CD and have improved long-term survival rates of IBD patients [13,20,21]. However, corticosteroids typically have a systemic distribution and induce serious side effects; thus, their use should be avoided in maintenance therapies and side effects should always be monitored during treatment. Side effects include loss of bone marrow, hyperglycaemia, psychosis, cataracts, impaired wound healing, osteoporosis, growth retardation in children and hypothalamic-pituitary-adrenal axis suppression, among many others, worsened with higher doses and prolonged administration times [18]. Notwithstanding, efforts have been made to increase corticosteroid efficacy and safety, which led to the second generation of these drugs. Budesonide is one of the best examples of second-generation glucocorticosteroids in IBD. It is characterized by a high topical activity and a low systemic distribution, decreasing the frequency or intensity of side effects [22].

In cases of severe disease, maintenance therapy or when corticosteroids are contraindicated, immunosuppressants and biological therapies should be considered [13]. Immunosuppressants such as azathioprine and methotrexate inhibit nucleic acid synthesis, leading to a decrease in T cell proliferation and cytokine production, ultimately suppressing immune response [23,24]. Immunosuppressants play an important role in patients who have become steroid dependent [25], although associated with potentially serious side effects [23,26]. Biological agents show a good capacity to induce and maintain remission [27,28], and are primarily monoclonal antibodies that target and specifically bind to TNF-α, integrins or interleukins, stopping proinflammatory cascades and its effects [29,30]. As expected, the major downside of these drugs are the side effects. Potential side effects include a higher risk of infection by virus, fungi, bacteria and opportunistic species (tuberculosis being one of the most notorious cases), skin disorders, higher frequency of heart failure, autoimmune disorders and demyelination [19,30,31].

Aminosalicylates are nonsteroidal anti-inflammatory drugs (NSAID) and have been the most used drugs in therapies for IBD, with 5-aminosalicylic acid (5-ASA) being the active moiety. Aminosalicylates can be administered in many forms and manage localized inflammation with few side effects, making them a versatile and safe option [32]. Despite its mode of action not being fully understood, some proposed mechanisms include inhibition of proinflammatory molecules like prostaglandins, leukotrienes and some cytokines, similarly to the activation of PPARγ [33]. 5-ASA has demonstrated high efficiency in the treatment

of mild to moderate UC although showing limited action in the treatment of CD. Nevertheless, it is still being prescribed to CD patients [34].

1.2. 5-aminosalicylic acid

5-aminosalicylic acid, commonly known as mesalazine, is the first line in step-up therapies of IBD and particularly effective in mild to moderate UC. Its prodrug sulfasalazine (or salazopyrin), consists of a sulfapyridine moiety coupled to 5-ASA by an azo bond (-N=N-) (**figure 1**), and has been known to be effective in UC treatment for over 70 years [35]. It was originally designed to target rheumatoid arthritis, which was thought to have a bacterial aetiology and sulphonamides were the first effective antibacterial drugs to be discovered [36]. However, it took near 60 years to consider 5-ASA as the drug moiety of choice to treat IBD, which happened due to the increased intolerance and allergy risk of the sulfapyridine group [17].

Sulfasalazine, as in all azo-bound prodrugs, is converted to 5-ASA in the colon. It is proposed that colonic bacterial enzymes are responsible for catalysing this reaction, although non-enzymatic reduction of azo-bonds has also been demonstrated [37]. Other 5-ASA azo bound prodrugs include olsalazine and balsalazide. While olsalazine is a 5-ASA dimer, *i.e.*, two 5-ASA molecules bound by an azo bond, the carrier moiety of balsalazide is 4-aminobenzoyl-β-alanine, an inert molecule. Although olsalazine is associated with an increased risk of diarrhoea, these prodrugs show a higher tolerance than sulfasalazine and with similar results in the of clinical remission in UC [38–40].

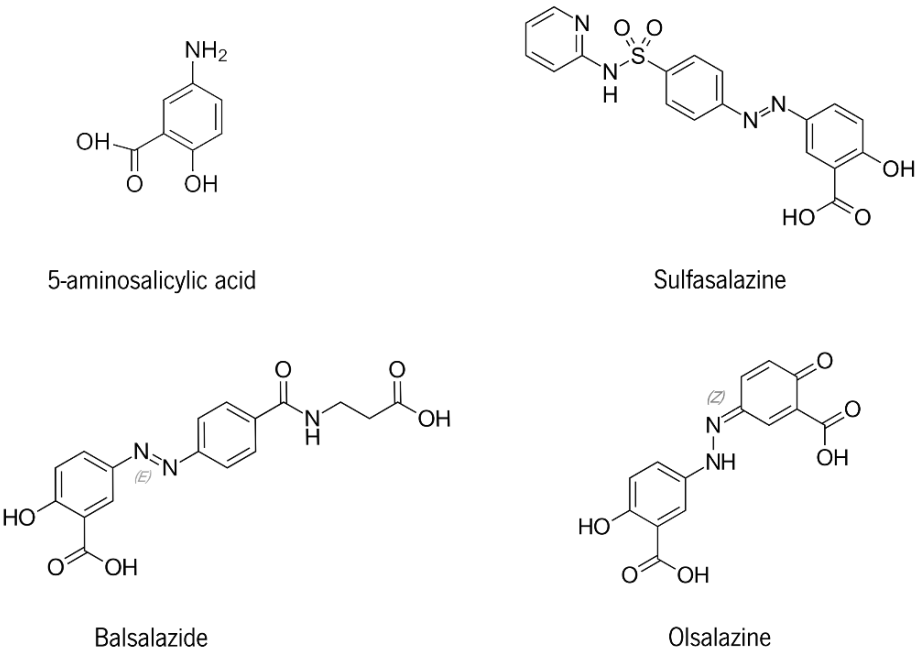

Figure 1 - Chemical structures of 5-ASA and its most common prodrugs.

1.2.1. Physicochemical and pharmacokinetic properties

The International Union of Pure and Applied Chemistry (IUPAC) nomenclature for 5-ASA is 5-amino-2-hydroxybenzoic acid. It has a molecular weight of 153.14 g/mol, 3 hydrogen bond donors and 4 hydrogen bond acceptors, and appears as odourless white to pinkish crystals or purplish-tan powder. Its solubility in water at 20 °C is 0.84 g/mL and it is insoluble in ethanol. It has 2 dissociation constants, with estimated pK_a values of 2.30 for the carboxyl group and 5.69 for the amine group [41]. At pH 7, such as in the intestinal environment, 5-ASA is in its monoanionic form, *i.e.*, with a net charge of -1 due to the loss of the carboxyl proton. In aqueous solutions, the monoanion ($HASA^-$), neutral (H_2ASA) and monocation (H_3ASA^+) forms of 5-ASA present absorption peaks at 332 nm, 298 nm and 303 nm respectively, showing high Stokes' shifts with emissions at 505 nm, 405 nm and 465 nm [42].

Without any delivery systems or unbound as a prodrug, most of 5-ASA is absorbed in the stomach and small intestine, meaning that only approximately 20 % of the administered dose reaches the terminal ileum and colon [43,44]. Upon absorption, 5-ASA can either be metabolized to N-acetyl-5-aminosalicylic acid by N-acetyltransferase (NAT), an inactive compound that is excreted by the kidneys or in the faeces, or is transported into the tissue where it will perform its action [44,45].

Low doses of 5-ASA typically show no effect in the clinical remission of IBD, comparing with high doses [46–48]. This dose-dependency can be explained by NAT metabolism. At low concentrations, 5-ASA is converted by NAT. At higher concentrations, NAT reaction rate is not high enough to convert all the absorbed 5-ASA, resulting in higher intestinal concentrations and consequently, increased pharmacological effect [45]. Interestingly, inflammation is linked to decreased 5-ASA metabolism, which can mean an increased drug efficacy in IBD patients that show higher inflammation. Thus, the use of NAT inhibitors in combination with this drug may represent a promising treatment approach [49]. Nevertheless, the concentration of 5-ASA reaches a point above which no significant improvements are observed, suggesting a saturation point. *In vivo*, an oral daily administration of 5-ASA in the range of 1.2 g to 2.4 g demonstrated to be correlated with rising concentrations in the rectal tissue, but no significant increase was observed from 2.4 g to 4.8 g [50]. Most likely, when the oral daily intake is 1.2 g and 2.4 g, the drug concentration in the intestine is kept above the NAT metabolism saturation point and its concentration in the tissue rises. Close to 2.4 g daily intake, the tissue concentration stabilizes due to saturation of mucosal transport and any free 5-ASA is metabolized to N-acetyl-5-ASA by the liver and excreted in the urine [44,45].

1.2.2. Clinical significance

Many theories have been proposed to describe the mode of action of 5-ASA; however, its underlying mechanisms of action are still not fully understood. Since it shares some structural and pharmacological properties with common NSAIDs such as acetylsalicylic acid (aspirin) and acetaminophen (paracetamol), it is likely that 5-ASA functions as an inhibitor of 5-lipoxygenase and cyclo-oxygenases enzymes (COX-1 and COX-2), thus preventing synthesis of prostaglandins and leukotrienes, which are involved in proinflammatory response [33,44,51,52]. Although both COX enzymes catalyse the same reactions, their functions are different: COX-1 synthesises prostaglandins essential for physiological functions, whereas COX-2 is inducible by proinflammatory cytokines, growth factors and tumour promoters in several cell types, playing a crucial role in tumour initiation, promotion and progression [51].

It is known that 5-ASA's action depends on more interactions other than COX inhibition. It is hypothesized that it leads to the activation of peroxisome proliferator-activated receptors gamma (PPARγ), which are highly expressed in the colonic epithelial cells, ultimately leading to an anti-inflammatory response that includes the decreased activation of Nuclear Factor-Kappa B (NF-κB), a nuclear transcription factor that plays an important role in the expression of proinflammatory genes such as cytokines, chemokines and adhesion molecules [53,54].

It is also possible that 5-ASA has immunosuppressive effects. It has been found capable of inhibiting T-cell proliferation and activation, and phagocytosis of polymorphonuclear leukocytes and macrophages [36]. **Figure 2** summarizes 5-ASA interactions in the intestinal epithelium.

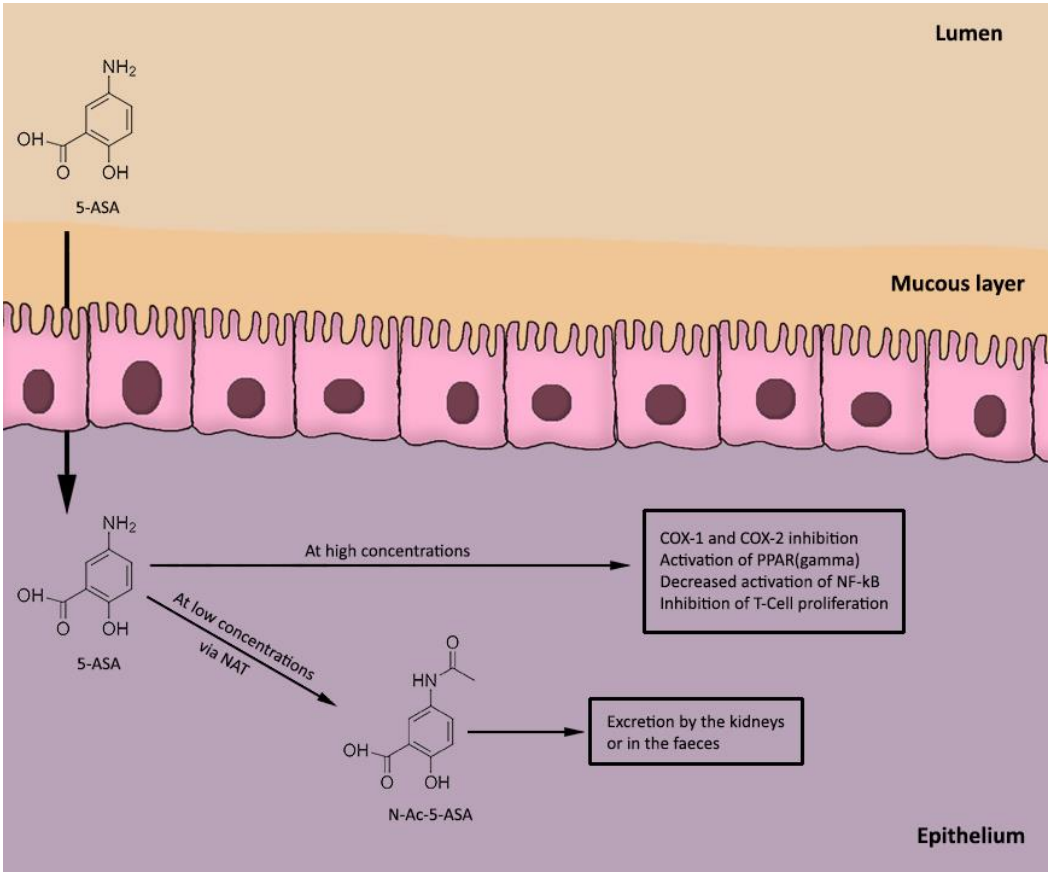

Figure 2 – Proposed 5-ASA anti-inflammatory mechanism and excretion. It is worth noting that NAT metabolism and subsequent excretion is a continuous process, even at high concentrations. The key difference stands in the fact that at high concentrations NAT conversion rate is not high enough to inactivate all 5-ASA in the epithelium.

Aminosalicylates, in general, demonstrate great results in mild to moderate UC and are typically the first medications to be prescribed in both forms of IBD. These can be administered in two major routes: orally or topically [13,55]. 5-ASA (and other aminosalicylates) shows a great capacity to not only induce remission, but also in preventing clinical relapse, while being well tolerated by UC patients, in either administration routes [39,46,56]. The topical administration of 5-ASA is typically employed in left-sided colitis, while the oral administration is applied to patients with more extensive disease. When prescribed to CD patients, 5-ASA seems to be able to maintain surgically-induced clinical remission [48], but has demonstrated to be ineffective in inducing remission [13,47,57].

The increased risk of developing CRC should be always considered in IBD therapies. 5-ASA has shown repeated evidence suggesting antineoplastic and inhibition of CRC cells proliferation caused by PPARγ activation, NF-κB dependent mechanisms (which may be a result of PPARγ activation) and COX-2 inhibition [51,58–60]. It is also reported that long-term administration of 5-ASA reduces transcription of cancer-associated genes [61]. This is a great advantage since CRC is one of the most serious conditions associated with both UC and CD. Another major advantage of using 5-ASA as therapeutic drug is the decreased frequency and seriousness of adverse effects. Mild side effects include dyspepsia, rash, headache and dizziness, while rare but more serious events include alveolitis, nephritis, pancreatitis and decreased fertility [17,44]. Moreover, the frequency of adverse events is low and often comparable to placebo [17,38,44].

In short, 5-ASA is still pointed as a viable treatment option in IBD patients, showing great results in mild to moderate UC, in the prevention of CRC, and presents a low frequency and seriousness of side effects.

1.2.3. 5-ASA drug carriers

Due to its attractive therapeutic properties, 5-ASA has received a lot of attention over the years. This led to continuous efforts in developing excipients and formulations in order to improve its pharmacokinetic properties, especially in controlling its release. Oral formulations in particular, must be designed to stay intact throughout the GIT and release the drug in the colon. In order to successfully achieve this, there are some physiological aspects that can be exploited such as pH, transit time and the intestinal microbiome [62]. pH-dependent formulations are amongst the most commonly used due to the pH differences throughout the GIT. While the stomach lumen is highly acidic, with a pH of 1-2 [63], the small intestine can present a wide range of pH values. At the proximal small intestine, it varies from 5.5 to 7 and, at the distal small intestine, it can range from 6.5 to 7.5 in healthy individuals and between 7 to 8 in IBD patients [64]. Finally, at the colon, pH can range from 5.5 to 7.5 in healthy individuals and from 2.3 to 7.3 in IBD patients [65]. This means that these kind of formulations can target a location within the GIT by dissolving at a specific pH For instance, the most common formulations dissolve at pH ≥ 6.5 or pH ≥ 7, typically starting to release the drug in the distal small intestine [65].

Regarding transit time, UC patients are reported to have shorter transit times than healthy individuals and with significant time variations [62,66]. This indicates that transit time is not an adequate approach for colon-targeted drug delivery, even though it should always be considered. As previously mentioned, the most common 5-ASA prodrugs are converted to its active form with the hydrolysis of the azo-bond by bacteria

from colon microbiota. Since most bacteria present in the colon are also capable of anaerobic fermentation of non-starch polysaccharides, which are typically not absorbed in the intestine, these have also been explored for the development of colon-specific drug delivery [67].

There are two main types of 5-ASA formulations: oral and topical/rectal. The most common oral formulations include pills and tablets made of polymers that dissolve in response to certain conditions, such as gastrointestinal pH or time in solution [33]. The most common examples of orally delivered 5-ASA formulations are Asacol® and Pentasa® tablets, which are made with Eudragit® and ethylcellulose respectively. Eudragit® is the brand name of a great number of polymethacrylate copolymers with the ability to dissolve at certain pH ranges, and it is found in many commercialized intestine-targeted formulations [68]. On the other hand, topical formulations typically consist in suppositories, suspensions and foams. While these can present great results when compared to oral formulations, patient compliance is lower due to discomfort and inconvenience [69,70].

Even with several different formulations on the market, research and development of novel 5-ASA drug carriers is still ongoing with the main goal to improve its effectiveness. Micro- and nanoparticulate delivery systems have been receiving a lot of attention in the past years for their attractive properties and ability to improve pharmacokinetics compared to conventional formulations [62]. Some relevant properties to be considered in these systems are size and surface charge [62]. Nano-scale carriers seem to selectively accumulate in inflamed tissue compared to healthy tissue in a size-dependent manner [71,72]. One proposed mechanism for this phenomenon is based on the higher number of antigen-presenting cells in inflamed tissue, which have the ability to phagocyte bacteria and smaller particles [71]. Surface charge also plays a role in the adhesion of particles in the colon. Positively charged particles adhere to the negatively charged mucins present in intestinal mucosa [62]. On the other hand, negatively charged particles adhere to the inflamed tissue due to a higher concentration of positively charged eosinophil proteins and transferrin; however, this is dependent on the ability of particles to penetrate into the mucous layer, which is associated with smaller particles [62]. Numerous micro- and nanoparticulate delivery systems have been proposed as vehicles for 5-ASA controlled release. The most relevant 5-ASA micro- and nanoparticle delivery systems are summarized in **table 2**.

Table 2 - Microparticulate and nanoparticulate systems for the controlled release of 5-ASA.

Material	Formulation	Release mechanism	Reference
SiO_2	Covalently bonded 5-ASA-SiO_2 nanoparticles	The small particle size is linked to an accumulation in inflamed tissue, where the bond is enzymatically degraded, releasing the drug	73,74
	Mesoporous silica microparticles	The mesoporous particles are loaded with hydrocortisone and the olsalazine groups at its surface prevent it from releasing; reaching the colon, olsalazine is hydrolysed and both drugs are release	75
	Diatom silica microparticles	5-ASA is released from the porous microparticles by diffusion	76
	SBA-16 silica nanoparticles coated with Eudragit® polymers	In colonic pH, the Eudragit® coatings dissolve, allowing the drug to diffuse from the pores to the colon	77
Chitosan	Chitosan-Ca-alginate microparticles	Chitosan is degraded by colonic bacteria and at pH ≥ 6.5 the complex slowly erodes, releasing the drug	78
	Thiolated chitosan-alginate mucoadhesive microparticles coated with Eudragit® S 100	The Eudragit® S 100 coating dissolves at pH ≥ 7, allowing the release to happen exclusively in the colon	79
	Chitosan nanoparticles loaded with hydroxypropyl-β-cyclodextrin/mesalazine inclusion complex	While chitosan is degraded in the colon, the inclusion complex slowly swells and prolongs the drug release	80
	Chitosan-carboxymethyl starch nanoparticles	The nanoparticles are eroded or degraded in the colon, slowly releasing the drug	81
	Rectally delivered chitosan microparticles	Upon rectal delivery, chitosan adheres to the mucosa and delivers the drug over the course of several hours	82
Acetylated inulin	Acetylated inulin microparticles	Inulin is a prebiotic degraded by colonic bacteria, releasing both SCFAs and the drug	83
Starch	Dissulfide-linked reduction-sensitive starch nanoparticles	It is estimated that the particles would be internalized by macrophages, releasing the drug	84

	Microcrystalline cellulose-starch microparticles coated with resistant starch films	The starch films are resistant to enzymatic degradation and erosion, allowing for a more prolonged release	85
Carboxymethyl cellulose	Carboxymethyl cellulose-rosin gum hybrid nanoparticles	5-ASA is released by diffusion with a combination of swelling and erosion	86
Xylan	Xylan-mesalazine nanoparticles	The xylan-mesalazine nanoparticles are degraded by colonic bacteria, releasing the drug	87
	Xylan-Eudragit® S 100 microparticles	Eudragit® S 100 dissolves in colonic pH releasing the drug	88
Acemannan	Acemannan-acrylonitrile nanoparticles	When in pH 7.4, the polymer matrix swells and slowly releases the drug	89
Eudragit® S 100	Eudragit® S 100 nanoparticles	Upon reaching the colon, Eudragit® S 100 dissolves and releases the drug	90
PCL	Mesalazine-PCL bound nanoparticles	Binding the drug to the polymer with a covalent bond allows for a more prolonged release in the site of action	91
PLGA	PLGA nanoparticles contained inside intestinal organoids	Organoids target inflamed tissue, where the PLGA nanoparticles release the drug	92
PLA	PLA microparticles	5-ASA is released by diffusion	93
Carbopol® 971	Carbopol® 971-poly(2-ethyl-2-oxazoline) complexes nanoparticles	It is hypothesized that in colonic pH, the hydrogen bonds between Carbopol® 971 and poly(2-ethyl-2-oxazoline) dissociate, releasing the drug	94

Silica-based systems

Silica-based micro and nanoparticles are commonly used excipient due to easiness of preparation, ability to be surface-modified and safe toxicological profiles [62]. For instance, surface-modified SiO_2 nanoparticles with covalently attached 5-ASA have shown great results by preferably accumulating in inflamed tissue compared to healthy tissue. An increased mucous production in the inflamed areas leads to a selective adhesion and the higher abundance of immune cells can grant a selective uptake of nanoparticles compared with healthy tissue, which can be the key to efficacy in CD treatment [73,74]. Recently, Teruel *et al*. reported the use of mesoporous silica microparticles for the dual delivery of olsalazine and hydrocortisone, showing great results as a colon-targeted therapy [75]. In this delivery system, olsalazine is bound to the surface of the microparticles while hydrocortisone is entrapped inside the pores. When the

azo-bond of olsalazine is hydrolysed by colonic bacteria, both 5-ASA and hydrocortisone are released, delivering the two drugs simultaneously. Reports also show that diatom silica microparticles are very effective in delivering 5-ASA and prednisone with low toxicity, allying all the above mentioned advantages with a cost-efficient and eco-friendly production [76]. Trendafilova *et al.* designed SBA-16 silica nanoparticles, a unique mesoporous system with suitable properties to target the delivery of 5-ASA to the colon [77]. These particles have 3D porous channels and when coated with Eudragit® methacrylates show adequate release profiles for colon-specific drug release.

Polymer-based systems

Methacrylate derivatives such as Eudragit® are amongst the most widely used polymers in 5-ASA delivery systems due to the pH-dependent dissolution. Several studies report the use of Eudragit®-based materials for the development of micro- and nanoparticle delivery systems. Eudragit® S 100 have been used for the preparation of nanoparticles able to encapsulate 5-ASA with a loading efficiency near 60 % [90]. This system presents the advantage of being dissolvable at pH ≥ 7, indicating its potential for colon-specific release. Other polymeric approaches involve the use of 5-ASA covalently bound to poly(ε-caprolactone) (PCL) nanoparticles, granting a slower release [91]. This system resists degradation in the GIT before reaching the colon and the polymeric nanoparticles are further degraded in the inflammation tissue due to uptake by immune cells, allowing a drug release specific to inflamed sections of the GIT. Notably, this strategy allowed a 60-times higher efficiency compared to both the control group and the physical drug entrapment [91]. Still, the major obstacle of this system is the very limited number of potential drug binding sites.

Another promising polymer is poly(lactic-co-glycolic acid) (PLGA) due to characteristics such as high deposition on inflamed regions and biodegradability. Organoids containing PLGA nanoparticles loaded with 5-ASA demonstrated to work as a Trojan horse against IBD, due to the preference of organoids to target inflamed tissue [92]. Moreover, organoids were shown to grow normally with and without the presence of PLGA nanoparticles, showing the biocompatible nature of the polymer. Although further studies are needed, this system shows great prospects in IBD treatment.

Poly(lactic acid) (PLA) has also been used to produce different microspheres capable of entrapping 5-ASA by varying the emulsifier concentration and the drug/polymer ratio, some of which were able to effectively entrap and release mesalazine [93]. More recently, the use of Carbopol® 971 and poly(2-ethyl-2-oxazoline) complexes have been proposed, which can self-assemble into nanoparticles capable to successfully

encapsulate 5-ASA and delay its release [94]. This novel formulation showed great variability depending on the polymer mixture and pH in which the system is prepared.

Polysaccharide-based systems

In addition to silica-based particle systems, a variety of polysaccharides have been also used for the production of micro and nanoparticle delivery systems. Chitosan, inulin, starch, cellulose, xylan and acemannan are amongst the polymers of choice as these are generally cheap, abundant, and biocompatible. Chitosan was one of the first polysaccharides to be used as microparticulate delivery system for 5-ASA, displaying mucoadhesive properties and the ability to be degraded by colonic bacteria, leading to colon-targeted delivery [95]. Mladenovska and co-workers reported the formulation of chitosan-Ca-alginate microparticles with mucoadhesive properties and the ability to be soluble only at pH higher than 6.5, preventing an early drug release [78]. Duan *et al.* developed a similar system with chitosan-alginate microparticles coated with Eudragit® S 100 for dual delivery of 5-ASA and curcumin [79]. In this system, the Eudragit® coating grants that the microparticles are released only at pH ≥ 7, which decreases the chances of an early release and possibly helps in mucoadhesion since chitosan is not eroded before reaching the colon. This system showed great results in mucosa adhesion and in alleviating inflammation in the colon of rats [79]. Chitosan nanoparticles have also been used in the loading of a hydroxypropyl-β-cyclodextrin/mesalazine inclusion complex [80]. Although no *in vivo* studies have been conducted with this system so far, *in vitro* anti-inflammatory tests have shown great results. Saboktakin *et al.* also produced chitosan nanoparticles by complex coacervation with carboxymethyl-starch, which occurs in pure aqueous environments and is ideal for maintaining the in-process drug stability [81]. Although micro and nanoparticles tend to be delivered orally, rectal delivery of mesalazine-loaded chitosan microparticles have also been formulated and shown retention lasting up to 48 hours, significant mucoadhesion and therapeutic efficacy with concentrations 2-fold lower than a commercially available formulation [82].

Inulin, a carbohydrate material consisting of linear β(2→1)-linked fructose units [96], has also been employed for the formulation of microparticle 5-ASA delivery systems [83]. As a prebiotic, inulin is degraded by colonic bacteria into short-chain fatty acids (SCFAs) like acetate, propionate and butyrate that promote intestinal health. The use of inulin for the delivery of 5-ASA is thus an interesting approach for colon-targeted release. Native inulin is hydrophilic and while inulin-based microparticles exhibit an early burst drug release, its acetylation demonstrated to increase the hydrophobicity with microparticles presenting a more prolonged release [83].

Native starch-based microparticles have been described as unsuitable for controlled release, mainly due to its high swelling in aqueous media and rapid enzymatic degradation, originating a fast release [97]. However, some works have demonstrated its potential as 5-ASA delivery system with some modifications. Yang *et al.* produced dissulfide-linked starch nanoparticles, making them reduction-sensitive [84]. These carriers demonstrated to be non-cytotoxic, biocompatible, biodegradable and with adequate size, showing potential as 5-ASA delivery system. More recently, microcrystalline cellulose cores loaded with 5-ASA were coated with resistant starch films, for colon-targeted delivery of existent microparticle systems [85].

Cellulose has also been considered as an option for novel 5-ASA formulations with the advantage of being an abundant and inexpensive source. Although its native form is water-insoluble, which is inadequate for micro or nanoparticle delivery systems, water-soluble chemical variants represent viable alternatives. For instance, carboxymethyl cellulose is an ionic, biocompatible and water-soluble polysaccharide with adequate properties for a 5-ASA drug delivery system, despite presenting some limitations for hydrophilic drug delivery [86]. Singh *et al.* designed a carboxymethyl cellulose-rosin gum hybrid nanoparticle capable of delivering 5-ASA, with the polymer network controlling the swelling ratio and consequently delaying the drug release [86].

Xylan, one of the most abundant polysaccharides found in plant cell walls, is another polysaccharide used for the formulation of new deliverable systems [87]. Kumar and co-workers successfully produced xylan-mesalazine conjugates that self-assemble into nanoparticles [87]. This system is degradable by colonic bacteria, granting a colon-specific and environmentally friendly nanoparticulate drug delivery system. Also, Silva *et al.* developed xylan/Eudragit® S100 hybrid microparticles by spray-drying, capable to encapsulate 5-ASA and releasing it at pH 7.4 due to the solubility of Eudragit® S100 [88].

Finally, poly(acrylonitrile) nanoparticles conjugated with acemannan – a water-soluble polysaccharide consisting of a combination of mannose, glucose and galactose extracted from aloe vera leaves – were developed by Malviya *et al.*, showing an efficient controlled pH-dependent release of 5-ASA [89].

1.3. Elastin-like recombinamers

Elastin is an extracellular matrix protein included in elastic fibres, which grants elasticity and resilience to several tissues including the skin, lungs and blood vessels and plays a key role in maintaining the normal functioning of these organs [98,99]. Over the past few decades, sequence and structure analysis of this protein revealed that repetitive sequences, abundant in proline (P), glycine (G) and valine (V) were common and had a major role in its properties [100]. In the early decade of 1990, the first attempts at producing elastin-like peptides relied on the synthesis of repeating sequences based on the previously mentioned amino acids: these not only granted flexible properties to other peptides [101] but also had an aggregating ability in peptides made exclusively from a repeating monomer based on those sequences [102]. This gave rise to a new type of biomaterials commonly referred as elastin-like recombinamers (ELR) or elastin-like polypeptides (ELPs).

ELR are genetically engineered polypeptides based on the repetition of the mammalian tropoelastin sequence VPGXG with X, the guest residue, being any natural amino acid except proline [103]. One of the most interesting and remarkable properties of these recombinant protein polymers is a reversible self-assembly ability dictated by a transition temperature (Tt), a process commonly referred as inverse temperature transition (ITT) [104,105]. In aqueous solutions this process allows for two different ELR organizations and solubility according to the temperature: in low temperatures, the polypeptides are dissolved whereas in high temperatures self-assembly occurs and ELR form insoluble micro- or nano-sized structures [105]. Below the Tt, due to hydrophobic hydration, ELR chains are hydrated with water molecules organized in a clathrate-like structures. Heating above the Tt leads to a phase transition, breaking down the clathrate-like water organization and exposing the polypeptide chains, allowing their self-aggregation in an entropically driven and reversible process [105,106]. The Tt is influenced by several different factors, either according to the nature of the ELR or the environmental conditions, meaning it can be appropriately designed in conformation with its intended applications. The Tt decreases as hydrophobicity increases which is mainly dependent on the repetitive sequence and chain size [105,106]. Common external factors that influence the self-assembly response include the ionic strength of the solution, concentration and pH [105,106]; for the latter, this is conditioned by the presence of a charged amino acid in the guest residue to confer pH sensitivity as a result of polarity changes between the protonated and deprotonated states. Nevertheless, the ability to be custom-designed by genetically engineering its structure through the DNA sequence allows to tailor-made its behaviour, adding functional groups that confer a stimuli response in the presence of other external factors [105,106].

The term recombinamers in the main nomenclature ELR highlights the oligomeric and recombinant nature of these biomaterials. Upon constructing the gene with the intended sequence, it is necessary to choose an expression system. *E. coli* is one of the most used, well-known and characterized organisms, which led to becoming the most common heterologous expression system of ELR [107]. Once produced, the polypeptides need to be purified, most commonly by taking advantage of ITT and the associated Tt, through a process designated Inverse Transition Cycling (ITC). Once above the Tt, the peptide chains undergo self-assembly, folding hydrophobically and aggregating in a phase-separated state, ultimately precipitating. Repeated cycles of heat-cold centrifugation and incubation steps result in a purified product [108].

A great advantage of ELR-based materials is the high versatility, *i.e.*, they can form a great number of different structures, with the most common being nanoparticles, hydrogels and fibres [105] and have many applications. As biomaterials, the potential for biological applications is very high due to its biocompatibility and thermal responsiveness. Various attempts have been made to formulate drug delivery system, with some notable examples like temperature-triggered depots, drug-ELR conjugates and functionalized ELR systems, which can be applied in many diseases from cancer to autoimmune disorders [104,109]. Tissue engineering is also an area of interest with reported efforts in cartilage, vascular graft, ocular and liver tissue, although ELR have limited loading capacity [105,110]. The self-assembly property can also be exploited for protein purification by using ELR as fusion proteins, facilitating the methodology required and with a low associated cost [105,111]. Functionalization of surfaces is also an area of interest, granting many properties combined with temperature-responsiveness [111]. ELR have the potential to be used in a broad range of areas and continued research and development is necessary to unfold more potential uses.

VPAVG is one of the repetitive sequences used as ELR. The substitution of the central glycine in the VPGVG sequence by an L-alanine (A), results in a protein polymer displaying the characteristic thermoresponsive behaviour of ELR, coupled with a thermal hysteresis – the polypeptide chains hydrophobically fold at temperatures above Tt but only dissociate when a strong undercooling is achieved. This behaviour has been associated with the presence of a methyl group in the alanine residue that provides a more perfectly stable folding state when compared to conventional poly(VPGVG) [112,113]. When heated above its Tt, poly(VPAVG) self-assembles into sub-microparticles, which allows the entrapment of bioactive molecules during the assembly process that can be used for drug delivery purposes [114–116]. The recombinant protein polymer A200, consisting of 200 repetitions of the VPAVG pentapeptide,

demonstrated to self-assemble at a temperature near 32 °C, resolubilizing only at a temperature of approximately 10 °C [112,113]. This allows the spontaneous formation of self-assembled structures above Tt, which are stable over a wide range of temperatures due to the thermal hysteresis. The self-assembling process of A200 demonstrated to be characterized by the formation of slightly ellipsoidal nanoparticles with a hydrodynamic radius ranging from 190 nm to 295 nm, and was able to successfully entrap bone morphogenetic proteins (BMPs) with an encapsulation efficiency over 94 % while releasing it in a sustained process [114].

A200-based nanoparticles have also been used as fusion carriers of antimicrobial peptides [117]. Hepcidin-A200, a protein polymer genetically engineered to incorporate the amino acid sequence for the antimicrobial peptide hepcidin, demonstrated antimicrobial properties against both gram-positive and gram-negative bacteria [117]. This approach presents not only the advantage of allowing for the seamless production and purification of antimicrobial peptides, but also provides a platform for the development of antimicrobial drug delivery systems [115].

1.4. Objectives

While a great number of 5-ASA formulations has been developed, its effectiveness is still limited in more severe disease and in CD. As a solution, this work proposes the use of ELR nanoparticles as a carrier for 5-ASA. ERLs, and specifically A200, has shown great potential as a controlled release drug carrier, combined with a mild and eco-friendly production and great biocompatibility.

The main goal of this thesis was to assess the feasibility of using a recombinant A200-based protein polymer as vehicle for the controlled release of 5-ASA in the gastrointestinal tract. The sequence for the recombinamer used in this work, named NCKA200, comprises a block of 200 repetitions of the pentapeptide VPAVG, flanked with three lysine (K) residues at the N- and C-terminal. In this work, NCKA200 is referred to as A200. To achieve the proposed goal, the work was divided in four main objectives:

1. Production and purification of A200 nanoparticles;

2. Characterization of the self-assembly process and the produced nanoparticles;

3. Development of a quantification method of the 5-ASA;

4. Determination of the loading parameters of 5-ASA in the A200 particles and evaluation of its cumulative release profile.

2. Materials and Methods

2.1. Biological material and culture media

Escherichia coli BL21(DE3) was used for protein production. This strain was previously cloned with the plasmid p10NCKA200 in the scope of previous works developed in our lab and was provided for the realisation of this study. The plasmid P10NCKA200 is a modified version of the expression vector PET25b(+) with substitution of the ampicillin resistance marker by kanamycin (kan), and contains the gene encoding for the protein of interest, consisting in 200 repetitions of the pentamer VPAVG flanked with a three lysine block at both the N- and C-terminus (**Annex I**). *E. coli* propagation from frozen stock cells was achieved in Lysogeny Broth (LB) agar medium (10 g tryptone, 5 g yeast extract, 5 g NaCl, 20 g agar, per litre), supplemented with 50 µg/mL kanamycin as selection marker. For protein production, cells were grown in Terrific Broth (TB) (12 g tryptone, 24 g yeast extract, 5 g glycerol, 0.17 M KH_2PO_4 and 0.72 M K_2HPO_4) supplemented with 2 g/L of lactose for auto-induction (TBlac) [118] and 50 µg/mL of kanamycin as selection marker.

2.2. Protein expression and purification

Before initiating the protein production, frozen *E. coli* cells harbouring p10NCKA200, stocked in glycerol, were refreshed two times in LB agar plates supplemented with kanamycin and allowed to grow overnight at 37 °C. Fresh cells were then used to inoculate TBlac + kan, with a volumetric ratio of 1:4 (e.g. 250 mL of medium in 1 L flasks) at 37 °C, under 200 rpm agitation, for 22 h. After fermentation, the optical density (OD) was measured at 600 nm. Then, cells were harvested by centrifugation at 5,807 x g, at 4 °C for 10 minutes, and frozen at -20 °C until purification.

For protein purification, cells were resuspended in Tris-EDTA (TE) buffer (50 mM Tris-HCl, 1 mM EDTA, pH 8.0), in a volume of 60 mL per pellet resultant of 1 L of fermentation, and lysed by ultrasonic disruption with a Vibra-Cell™ 75043 (Bioblock Scientific, 750W max power) sonicator, using a 25 mm diameter probe. Sonication was performed with an amplitude of 60 %, alternating between pulses of 3 s on and 9 s off, for a total sonication time of 10 min. Samples were kept on ice throughout the entire lysis process. After disruption, the pH of the cell crude extract was adjusted to 3.5 with HCl 1.6 M and agitated for 30 minutes at 4 °C. After sonication and acidification, the lysate was centrifuged at 10,695 x g, for 20 min at 4 °C for removal of insoluble debris. The clear supernatant was carefully collected to new tubes and

used for purification by ITC, which allows the purification of the recombinant protein by sequential heating and cooling cycles, resulting in precipitation and resolubilization respectively (**figure 3**). The initial step comprised a heating stage by incubation at 37 °C for 3 h, followed by a centrifugation at 10,695 x g, at 37 °C for 20 min. Due to the self-assembly and precipitation of A200, the protein is retained in the pelleted fraction. The pellet was resuspended in the same volume of cold ultra-pure water and left at 4 °C for 3 hours, allowing the protein polymer to resolubilize. To finish the first ITC cycle, the resolubilized fraction was then centrifuged at 10,695 x g for 20 min at 4 °C, and the pellet discarded. Additional heating/cooling cycles were performed using the same abovementioned conditions, with the exception that 0.1 M NaCl was added at the start of every heating step. Once all the ITC cycles are finished, the protein-enriched sample was dialysed against water to remove salts (10 kDa – 12 kDa membrane, Medicell Membranes Ltd) and centrifuged at 10,695 x g for 20 min at 4 °C to discard insoluble debris. The resulting solution was frozen at -80 °C and lyophilized by freeze-drying (Christ Alpha 2-4 LD Plus, Bioblock Scientific).

2.3. SDS-PAGE

Sodium dodecyl sulphate polyacrylamide gel electrophoresis (SDS-PAGE) was employed to evaluate protein expression levels in bacterial cells after fermentation, as well as to monitor the purification process. In all cases, SDS-PAGE analysis was performed using 10 % polyacrylamide gels (**Annex II**) and ran with a voltage of 15 mA per gel. For evaluation of protein expression levels in bacterial cells after fermentation, samples were normalized to an equivalent OD_{600} of 0.1 according to the following formula:

Eq. 1 $$OD_{600} \times V_w = 0.1 \times 125\ \mu L$$

Where OD_{600} is the optical density (OD) of the bacterial cell culture measured at 600 nm, V_W is the volume to be loaded, 0.1 is the normalized OD and 125 µL is the volume of each sample (100 µL of sample + 25 µL of loading buffer 5 X concentrated, **Annex II**).

Gels were stained with a freshly prepared 0.3 M $CuCl_2$ solution and images were acquired with a Molecular Imager ChemiDoc XRS system. For Coomassie blue staining, the $CuCl_2$-stained gels were destained with TE buffer 10 X and stained with Coomassie blue (**Annex II**).

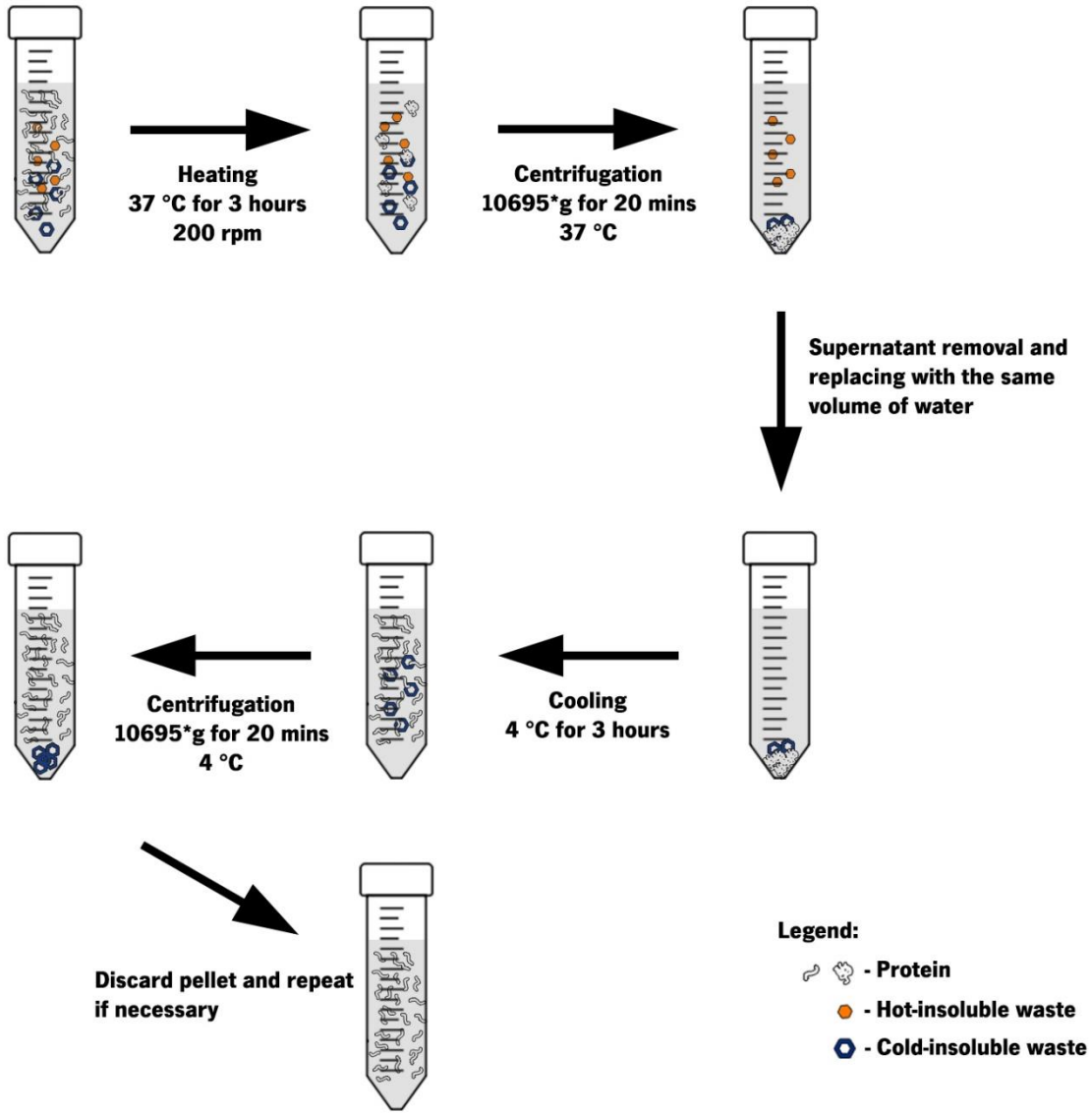

Figure 3 - Schematic representation of protein purification by ITC.

2.4. Characterization of the self-assembly

2.4.1. Determination of the transition temperatures

Differential Scanning Calorimetry (DSC) was used to identify the temperatures at which the self-assemble particles are formed (Tt) and at which the particles resolubilize (Ts). Two solutions of A200 at a concentration of 25 g/L, one in dH_2O and one in PBS (8 g of NaCl, 0.2 g of KCl, 1.44 g of Na_2HPO_4, 0.24 g of KH_2PO_4, pH 7.4) were used for DSC analysis in a Mettler Toledo DSC822e. For each DSC run, 25 µL of sample was placed in a hermitically sealed aluminium pan and subjected to thermal analysis in a four-

stage temperature program (**figure 4**): i) an isothermal stage, where the sample is maintained at 0 °C for 5 minutes; ii) a heating stage (HS) from 0 °C to 50 °C at a constant rate of 5 °C/min; iii) an isothermal stage, where the sample is maintained at 50 °C for 5 minutes; iv) a cooling stage (CS) from 50 °C to 0 °C at a constant rate of -5 °C/min. Thermogram analysis was completed using STARe™ Evaluation Software.

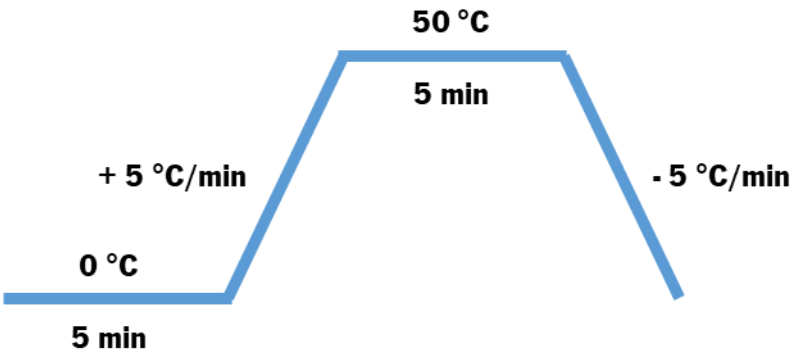

Figure 4 - Representation of the temperature program used for DSC analysis.

2.4.2. Particle size distribution and surface charge

The determination of particle size and zeta potential was achieved by Dynamic Light Scattering (DLS) and Electrophoretic Light Scattering (ELS) using a Zetasizer Nano Series (Malvern, UK). DLS analysis was carried out at 37 °C using A200 solutions (0.05 g/L and 0.1 g/L) in PBS or ultra-pure water. Size measurements were carried out using a refractive index (RI) of 1.45 for the material. For water solutions, RI and viscosity values were set to 1.330 and 0.5482 cP, respectively; for PBS solutions, the RI and viscosity values were set to 1.332 and 0.6875 cP, respectively. Before initiating the measurements, samples were subjected to an equilibration time of 180 s once the desired temperature was achieved. A total of 5 measurements per sample were performed, detected at a 173° angle (backscatter). For ELS, in addition to the previously established conditions, the dielectric constant was set to 70.2 for water and 74.4 for PBS. Due to the high conductivity of the PBS solution, the analysis model used was monomodal, with a voltage of 40 V. All samples were measured 5 times, with a minimum of 10 runs and a maximum of 100 runs.

2.4.3. SEM analysis

To evaluate the morphology of the particles and its size, the samples were visualized using Scanning Electron Microscopy (SEM). Unloaded and 5-ASA-loaded A200 self-assembled particles were prepared as described in section 2.5 and coated with a thin Au/Pd (gold/palladium) layer using a sputter coater and visualized in a NanoSEM FEI Nova 200. Mean particle size of 20 random particles was calculated with ImageJ software [119].

2.5. Quantification of 5-ASA by absorbance and fluorescence

Absorbance and fluorescence spectroscopy were used to quantify 5-ASA in all solutions, specifically for the drug entrapment and release assays. The first step was to acquire the absorbance and fluorescence spectra of 5-ASA for determination of the calibration curve. For all measurements, solutions were prepared with 5-ASA 99% (ACROS Organics™) in PBS pH 7.4 and read in 96-well microplates (200 µL) in a Tecan i-control Infinite 200 Pro microplate reader.

2.5.1. Absorbance spectrum and calibration curve

For the absorbance spectrum, an initial reading over the range of 280 nm to 800 nm was acquired using optically transparent Nunc™ polystyrene 96-well plates (Thermo Fischer Scientific). Once the spectrum was acquired, the absorption peak was identified and a calibration curve was created using ten different concentrations of 5-ASA, ranging from 0.03 g/L to 0.3 g/L. The calibration curve was created from the average of nine readings for each concentration of 5-ASA and a linear regression was applied.

2.5.2. Fluorescence spectrum and calibration curve

Fluorescence readings were performed in black Nunc™ polystyrene 96-well microplates (Thermo Fischer Scientific). Prior to data acquisition, the parameters of the fluorescence protocol in the microplate reader were optimized to yield consistent readings. The optimized parameters were the gain and the height of the objective above the sample (Z-position). The gain was calculated for the highest concentration sample and the Z-position was determined by the max ratio between the fluorescence intensities of a sample and the blank. For acquisition of the fluorescence spectrum, the excitation wavelength was fixed at 300 nm

and an initial emission sweep was performed from 330 nm to 800 nm. The emission peak was identified and used for the creation of a calibration curve using 12 different concentrations of 5-ASA, ranging from 1.5625 x 10^{-4} g/L to 0.01 g/L. The calibration curve was created from the average of nine readings for each concentration and a linear regression was applied.

2.6. Drug loading and release

2.6.1. Drug loading

Encapsulation/loading of 5-ASA was achieved by exploring the spontaneous self-assembly behaviour of the ELR in an aqueous solution. An initial optimization protocol was devised to determine the optimal combination of the 5-ASA and A200 concentration. Five different 5-ASA concentrations, selected based on literature [80], and three different A200 concentrations were combined for a total of fifteen different combinations (**table 3**).

Table 3 – Combinatorial design with letter-number codification used for the initial optimization studies. A letter code was attributed to the different ELR concentrations, from A to C in decreasing order. A number code was attributed to the different 5-ASA concentrations, from 1 to 5 in decreasing order.

[5-ASA] (g/L) / **[NCKA200] (g/L)**	**0.2500 (1)**	**0.1875 (2)**	**0.1250 (3)**	**0.0938 (4)**	**0.0625 (5)**
10 (A)	A1	A2	A3	A4	A5
5 (B)	B1	B2	B3	B4	B5
2.5 (C)	C1	C2	C3	C4	C5

Stock solutions of 5-ASA (0.5 g/L) and A200 (20 g/L) were prepared in PBS pH 7.4 and maintained at 4 °C overnight to ensure complete dissolution. Due to the possible photodegradation of 5-ASA, all solutions were protected from light as much as possible. For encapsulation purposes, the stock solutions were used to prepare mixed solutions (A200 + 5-ASA) with adequate concentrations of each component, as represented in **table 3**, for a final volume of 750 µL. The samples were then incubated at 37 °C for 1 h at 200 rpm to promote the self-assembly of A200 and consequently, the entrapment of 5-ASA. The self-assembled particles were collected by centrifugation at 17,000 x g for 5 min and the supernatants

transferred to new tubes. The absorbance of the supernatants was acquired at 332 nm and used for the determination of unloaded 5-ASA by application of the calibration curve. The amount of loaded drug was calculated using the following mathematical formula and expressed as a result of four independent assays, each in triplicate:

Eq. 2 $$m_{loaded} = m_i - m_{unloaded}$$

Where m_{loaded} is the amount of loaded drug (in mg), m_i is the initial amount of 5-ASA in solution (in mg) and $m_{unloaded}$ is the amount of 5-ASA in the supernatant (in mg).

Determination of the loading parameters namely, encapsulation efficiency (EE) and average loading capacity (LC) was assessed after four independent encapsulation assays, each in triplicate. The EE is a measure of the amount of encapsulated drug relatively to the initial amount of drug and was calculated following **equation 3**. LC corresponds to the amount of loaded drug per milligram of particles and was determined by application of **equation 4**. The amount of 5-ASA was calculated by application of the calibration curve.

Eq. 3 $$EE(\%) = \frac{Initial\ 5\text{-}ASA\ concentration - Free\ 5\text{-}ASA\ concentration}{Initial\ 5\text{-}ASA\ concentration} \times 100$$

Eq. 4 $$LC(\%) = \frac{m(5\text{-}ASA\ loaded)}{m(A200\ particles)} \times 100$$

Where m(5-ASA loaded) is the amount of loaded 5-ASA (in mg), and m(A200 particles) is the amount of A200 (in mg).

2.6.2. Cumulative drug release

For the drug release studies, particles loaded with 5-ASA were prepared by inducing the spontaneous self-assembly at 37 °C and collected by centrifugation, as described above. Then, 1 mL of warm PBS pH 7.4 was added to the pelleted A200/5-ASA formulation and carefully mixed to allow particle dispersion. The samples were then placed in an incubator for 48 h at 37 °C and 200 rpm and time points were

collected after 1 h, 2 h, 4 h, 8 h, 24 h and 48 h of incubation. For the collection of samples throughout time points, the tubes were centrifuged at 17,000 x g for 1 minute and 200 µL of the supernatant was transferred to new tubes, replacing the same volume with warm PBS. Samples were then stored at -20 °C until analysis. For cumulative drug release, the amount of 5-ASA at each time point was determined by acquiring the fluorescence intensity at 504 nm with an excitation wavelength of 300 nm, followed by application of the calibration curve. Cumulative drug release was calculated using the following mathematical formula using experimental data from four independent assays, each in triplicate:

Eq. 5 $$CR_n\ (\%) = \frac{m_n + \sum_{i=1}^{n-1} mr_i}{m(\text{5-}ASA\ loaded)} \times 100$$

Where CR_n (%) is the percentage of cumulative release at the time point n, m_n is the mass of released 5-ASA (in mg) at the time point *n* – calculated by multiplying the concentration by the volume of 1 mL – and mr_i is the mass of 5-ASA (in mg) removed from all the previous time point samples – obtained by multiplying the obtained concentration by 200 µL.

A schematic representation of cumulative drug release determination is provided in **figure 5**. To study the kinetics of drug release, the data obtained from the cumulative drug release experiments were analysed using DDSolver, an Excel add-in software package used for dissolution data analysis [120]. DDSolver was used to select the kinetic model that best fits the obtained results. The tested models were zero-order, first-order, first order with Fmax, first order with Fmax and Tlag, Higuchi, Hixton-Crowel, Korsmeyer-Peppas, Korsmeyer-Peppas with F0 and Korsmeyer-Peppas with Tlag (**table 4**). The adjusted coefficient of determination (AdR^2), Akaike Information Criterion (AIC) and Model Selection Criterion (MSC) were automatically calculated by the software and used as the main optimization parameters to select the model that best fitted the drug release mechanism.

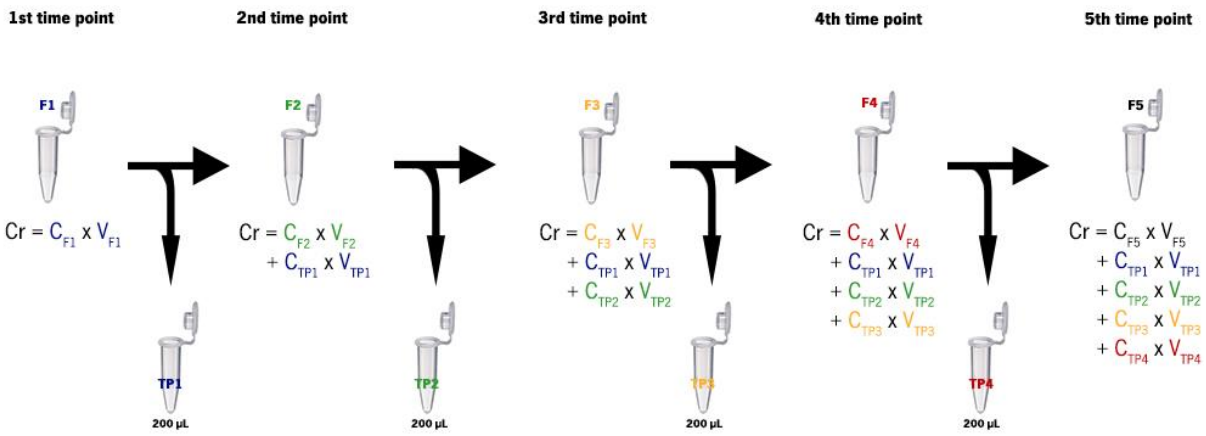

Figure 5 – Schematic representation of the methodology used for cumulative release assessment. Cr is the amount (in mg) of 5-ASA released up to that point, C_{Fn} and C_{TPn} are the concentrations (in mg/mL) at a given time point *n* (C_{Fn} = C_{TPn} for the same *n*), V_{Fn} is the volume of the working solution at the point *n* (1 mL) and V_{TPn}, is the volume of the sample taken at the time point *n* (200 µL). Colours were assigned according to the number of the time point.

Table 4 – Drug release kinetic models and respective mathematical expressions.

Model	Equation
Zero-order	$F = k_0 \cdot t$
First-order	$F = 100 \cdot (1 - e^{-k_1 \cdot t})$
First order with Fmax	$F = F_{max} \cdot (1 - e^{-k_1 \cdot t})$
First order with Fmax and Tlag	$F = F_{max} \cdot [1 - e^{-k_1 \cdot (t - Tlag)}]$
Higuchi	$F = k_H \cdot t^{0.5}$
Hixton-Crowell	$F = 100 \cdot [1 - (1 - k_{HC} \cdot t)^3]$
Korsmeyer-Peppas	$F = k_{KP} \cdot t^n$
Korsmeyer-Peppas with F0	$F = F0 + k_{KP} \cdot t^n$
Korsmeyer-Peppas with Tlag	$F = k_{KP} \cdot (t - T_{lag})^n$

F represents the fraction (%) of drug released at time t; k0 is the zero-order release constant; k1 is the first-order release constant; Fmax is the maximum fraction of drug released at infinite; Tlag is the lag time preceding drug release; kH is the release constant for the Higuchi model; kHC is the release constant for the Hixton-Crowell model; kKP is the release constant for the Korsmeyer-Peppas model; n is the diffusional exponent; F0 is the fraction for the initial burst release.

2.7. ATR-FTIR analysis

Attenuated total reflectance Fourier transform infrared spectroscopy (ATR-FTIR) was used as a complementary technique to evaluate the presence of 5-ASA in the self-assembled NCKA200 particles. A total of three samples were analysed: pure 5-ASA, empty A200 particles and particles loaded with 5-ASA. A200 particles were prepared by inducing the self-assembly process in PBS with and without 5-ASA, followed by centrifugation 17,000 x g for 5 min. The supernatant was carefully removed, and the pelleted particles were dried overnight at 37 °C, in the dark. ATR-FTIR analysis was conducted in a Spectrum Two FT-IR Spectrometer with deuterated triglycine sulfate detector and KBr beam spitter, coupled with a single reflection diamond UATR accessory (Perkin Elmer). FTIR spectra were collected at room temperature and represented as the accumulation of 64 scans with a resolution of 4 cm^{-1} from 4000 cm^{-1} to 400 cm^{-1}.

3. Results and discussion

3.1. ELR production and purification

The temperature-dependent behaviour of ELR is an attractive property due to the thermoresponsive behaviour upon thermal stimulus. In this work, A200 was selected as protein polymer to evaluate its feasibility as a drug delivery system for the release of 5-ASA. In addition to the self-assembly behaviour, resulting in the spontaneous formation of spherical sub-microparticles, A200 also exhibits a thermal hysteresis [113–115]. This allows the formation of self-assembled structures that are stable over a range of temperatures avoiding the use of additional stabilization methods (e.g., by chemical crosslinking) [117,121,122].

The protein polymer was produced in *E. coli* following the procedures previously described and purified using a protocol optimized by the group. After fermentation, bacterial cells were lysed by ultrasonic disruption to release the cytoplasmic content, and the pH was adjusted to 3.5 to precipitate native *E. coli* proteins and help in unaccomplished cell lysis. Centrifugation of the acidified lysate allows the recovery of A200 in the supernatant (**figure 6a**) whilst bacterial endogenous proteins remain in the pelleted fraction. This acidification step (**figure 6a**, lane **2**) demonstrated to be highly effective in the removal of a large amount *E. coli* contaminating proteins comparing with the crude cell extract (**figure 6a,** lane **1**). Further recovery of the protein polymer was achieved by ITC. As demonstrated in **figure 6b**, purification by ITC allowed the full recovery of the recombinant protein, resulting in a pure protein fraction by the end

of the process (**figure 6b**, lane 9). This matches the protein temperature-dependent property: during the cooling cycles A200 is soluble and, therefore, it is present in the supernatant. Contrarily, during the heating cycles, it self-assembles, aggregates and precipitates, remaining in the pelleted fraction after centrifugation. Successive cycles further increase the purification efficiency. Analysis of SDS-PAGE gels with Coomassie blue staining further supported the presence of ELR at the expected molecular weight. It is well known that ELR do not stain or stain very poorly with Coomassie [113,123], possibly due to the low amount of charged and aromatic amino acids. Moreover, the abnormal gel mobility at higher molecular weights is attributed to the hydrophobic nature of the recombinant protein and has been previously observed for other ERLs [113,124,125]. By the end of the purification process involving two ITC cycles, 49.54 mg of recombinant protein were obtained per litre of production media.

Overall, purification by ITC allowed a high recovery of A200, with no detected protein losses during purification steps, employing a relatively simple, "green" and inexpensive protocol.

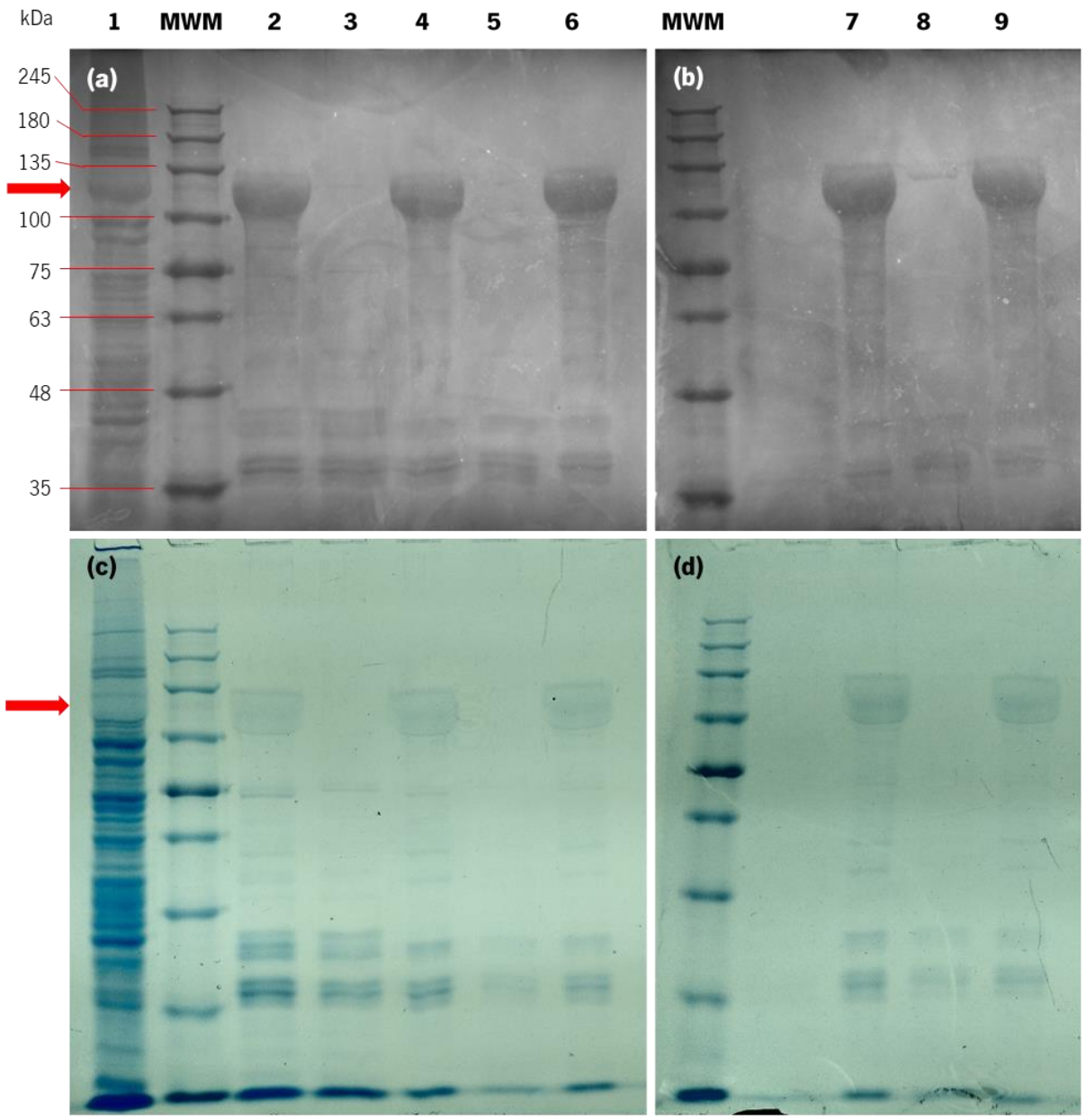

Figure 6 - SDS-PAGE gels representing the purification of A200 by ITC. Gels were stained with (a, b) $CuCl_2$ and (c, d) Coomassie blue. The red arrow points to the protein band corresponding to A200. Lane 1 – cell crude extract; lane 2 – supernatant after sonication and acidification; lane 3 – supernatant of the 1st heating cycle; lane 4 – pellet of the 1st heating cycle; lane 5 – pellet of the 1st cooling cycle; lane 6 – supernatant of the 1st cooling cycle; lane 7 – supernatant of the 2nd heating cycle; lane 8 – pellet of the 2nd cooling cycle; lane 9 – supernatant of the 2nd cooling cycle. MWM – molecular weight marker (NZYColour Protein Marker II).

3.2. ELR characterization

3.2.1. Thermal transition properties

DSC analysis was performed on A200 solutions, in PBS and in ultra-pure water, in order to determine the Tt – the temperature at which occurs the self-assembly – as well as the Td – the temperature at which the self-assembled A200 disassembles due to the reversibility of the process. Solutions with different ionic strengths – PBS and water – were used to assess differences in the transition and dissolution temperatures by comparing the different thermal events. **Figure 7** shows the thermograms of the DSC analyses obtained during the heating and cooling stages.

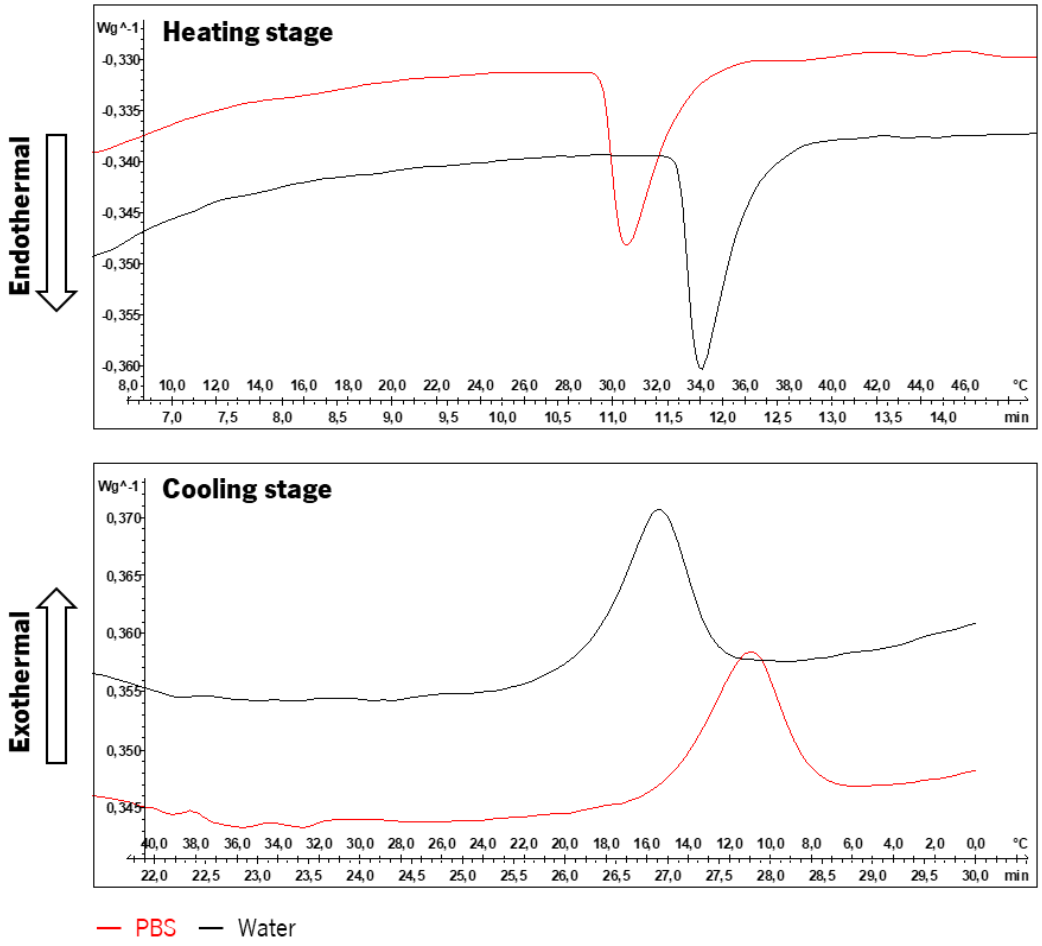

Figure 7 - DSC thermograms obtained for A200 samples in water (black) or PBS (red) solutions. The endothermic peak during the heating stage relates with the phase transition from the soluble to the insoluble state (self-assembly) and corresponds to the Tt. The exothermic event during the cooling stage relates with the resolubilization of the self-assembled protein polymer and corresponds to the dissolution temperature Td.

In the heating stage, as soon as a specific threshold is reached – the Tt – the ELR spontaneous self-assembles in an endothermic process driven by hydrophobic folding and disruption of ordered water structures [112,113,126]. According to Gibbs free energy, this process occurs mainly due to entropic factors and it can be explained by an increase in solvent entropy in combination with favourable interchain interactions [106]. In the cooling stage, once the Td is reached, the ELR polypeptide chains unfold and rehydrate in an exothermic process, accompanied by the reorganization of the solvent molecules in clathrate-like structures surrounding the polymer chain. In this work, the Tt and Ts were determined as the peak temperature of each event. The Tt for the samples in PBS and samples in water are of 30.51 °C and 33.91 °C, respectively, whereas the Td was determined to be 11.06 °C and 15.57 °C for samples in PBS and water, respectively (**table 5**).

Table 5 - Values of Tt and Td for the A200 samples in water and in PBS, calculated from the peaks of the DSC run.

Conditions	**Tt** (°C)	**Td** (°C)
A200 in PBS	30.5	11.1
A200 in Water	33.9	15.6

As observed, A200 in PBS present lower values for both Tt and Td than the experimental results obtained with A200 dissolved in water. This indicates that the higher ionic strength of PBS interferes with the self-assembling process by lowering the Tt, which is also observed for other ELR [117,126,127]. This can be explained by the increase in solvent polarity due to the presence of NaCl that results in a better formation of water structures surrounding the hydrophobic moieties of the polymer chain in the extended state [113,126,128]. The presence of salt is thus equivalent to an increase in the hydrophobicity of the polymer, acting as a "stabilizer" for water molecules and strengthens the intramolecular interactions of the hydrophobic folding, resulting in lower Tt [113,126,128].

Typically, the composition of ELR relies on the pentapeptide sequence VPGXG. In the present work, a variant of the traditional VPGVG sequence was used, by substituting the central glycine by an L-alanine. This substitution results in a protein polymer exhibiting a thermal hysteresis, as a consequence of the additional methyl group in L-alanine, which allows a more stable folding and hinders its unfolding [112,113]. The hysteresis behaviour of A200 is very attractive when considering its applications for drug delivery, as the self-assembled structures are stable over a wide range of temperatures without the need of further

stabilizing agents, *e.g.* by cross-linkers [114,116,117], possibly facilitating both storage and administration of potential future drug formulations.

3.2.2. Particle size and surface charge

The size and surface charge of the self-assembled structures was analysed by DLS and ELS. Light scattering allows to measure particle size through the Stokes-Einstein equation, which establishes a relation between particle movement and the hydrodynamic radius, based in the principle of Brownian motion. **Figure 8** shows the size distributions obtained for the samples dissolved in PBS or ultra-pure water at two different concentrations (0.05 g/L and 0.1 g/L). The mean diameter (Z-average) and polydispersity index (PDI) are presented in **table 6**.

Size measurements with ultra-pure water demonstrated a population of particles with average size increasing with concentration: from 89 nm with a concentration of 0.05 g/L, to 150 nm with a concentration of 0.1 g/L. This suggests an aggregation profile with increasing concentration. As for the samples in PBS, DLS measurements revealed an aggregation profile even at the lowest concentration, with around a 10-fold increase in average size compared with water: 1134 nm and 1681 nm for 0.05 g/L and 0.1 g/L. This aggregation behaviour was previously observed for A200 functionalized with antimicrobial peptides and attributed to the higher ionic strength of PBS [117,125]. Presumably, the higher ionic strength induces the already self-assembled structures to adopt a more compact conformation in the form of microaggregates [125,127].

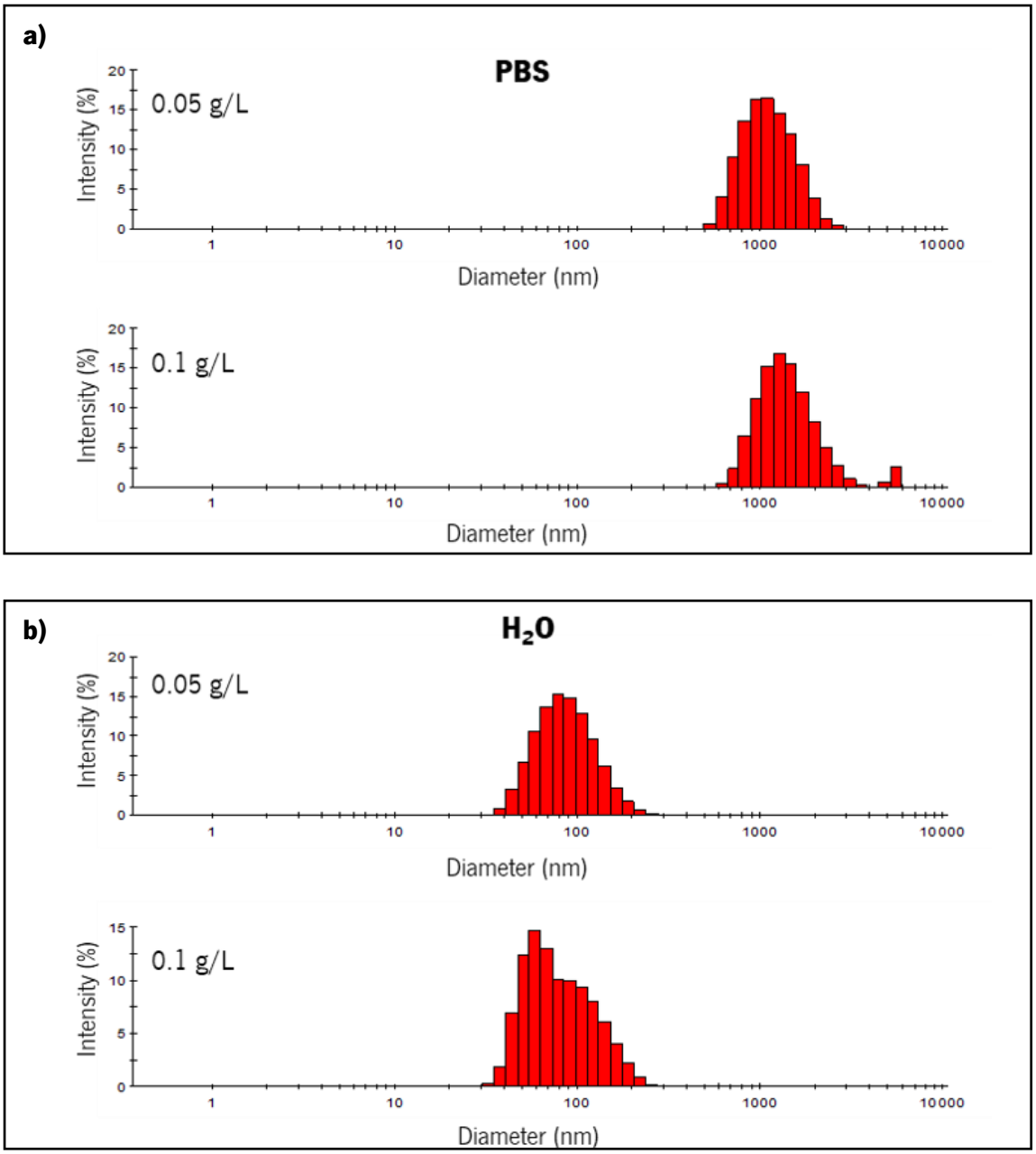

Figure 8 – Size distribution histograms of A200 at different concentrations in a) PBS and b) ultra-pure water (H_2O) obtained by dynamic light scattering at 37 °C.

Zeta potential measurements were performed for an estimation of surface charge in the self-assembled particles. A200 contains three lysine residues at both the N- and C-terminals and its pKa values are 2.18, 8.95 and 10.53 for the carboxylic acid group, the amine group and the side chain group, respectively [129]. This means that at neutral pH, lysine residues are positively charged and, in principle, this would result in differences in zeta potential.

Table 6 – Mean size (Z-average) and polydispersity index (PDI) values of A200 in PBS at 37 °C and A200 in water at 37 °C analysed by dynamic light scattering.

	Concentration (g/L)	Z-average (nm)	PDI
PBS	0.05	1134 ± 266	0.154
37 °C	0.1	1680 ± 454	0.252
H_2O	0.05	89 ± 4	0.198
37 °C	0.1	148 ± 135	0.193

Analysis of the particles' zeta potential revealed near-zero values for the water samples, +0.236 and +0.706 mV for the concentrations of 0.05 g/L and 0.1 g/L, respectively (**table 7**). As for the PBS samples, the zeta potential was slightly negative showing values of -3.89 and -5.81 mV for the concentrations of 0.05 g/L and 0.1 g/L, respectively (**table 7**). Previous works with ELPs have shown two possible folding mechanisms dependent of the arrangement of hydrophilic and hydrophobic blocks [130] (**figure 9**). ELPs with longer hydrophilic blocks, *i.e.*, 60 repetitions of the hydrophilic sequence and 200 repetitions of the hydrophobic sequence, fold with the hydrophilic fraction located in the surface of the particles. On the other hand, ELPs with shorter hydrophilic blocks, *i.e.*, 30 repetitions of the hydrophilic sequence and 200 repetitions of the hydrophobic sequence are not capable of forming this hydrophilic corona and instead remain on the inside of the particle [130].

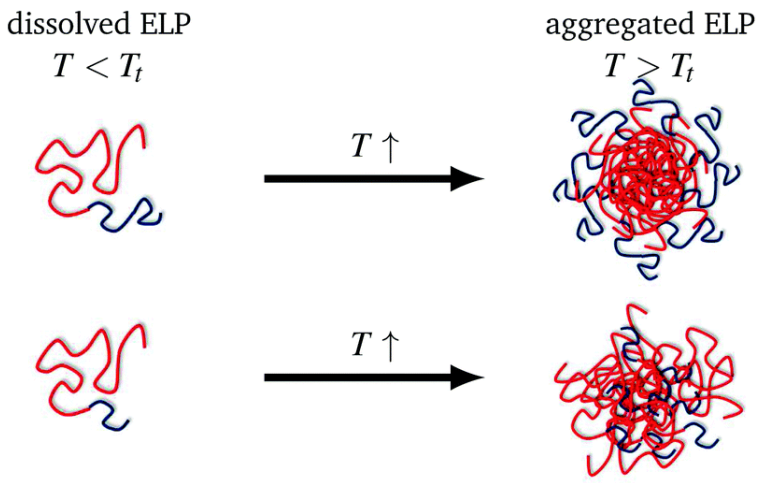

Figure 9 – Schematic representation of the different aggregation mechanisms for diblocks comprising 200 repetitions of hydrophobic sequence (in **red**) and 60 (top) or 30 (bottom) repetitions of the hydrophilic block (in **blue**). Reproduced with permission from Widder *et al.* (2017) [130].

In A200, the positively charged lysine residues constitute the hydrophilic part and are in a very small proportion compared to the hydrophobic part. Accordingly, the lysine residues are possibly inside the particles with no preferred arrangement, in an intertwined mesh-like structure, which supports the obtained zeta potential values. This could present a viable opportunity to encapsulate negatively charged drugs within the particles, which is the case for 5-ASA at pH 7.4. It is worth noting that the negatives values from the particles in PBS, even though close to zero, could indicate a different conformation of the particles when present in solutions with higher ionic strength but conclusions cannot be drawn from these results alone.

Table 7 – Zeta potential values obtained for the samples in PBS and water, obtained via the Zetasizer software.

	Concentration (g/L)	**Zeta potential (mV)**
PBS 37 °C	0.05	-3.89 ± 3.71
	0.1	-5.81 ± 4.01
H_2O 37 °C	0.05	+0.24 ± 1.10
	0.1	+0.706 ± 0.802

3.3. Determination of calibration curves

Typical 5-ASA detection and quantification is done either by absorbance spectroscopy or high-performance liquid chromatography (HPLC) [74–76,90]. While the prior is a simple an easy process, the latter requires relatively expensive and specific columns and the pre-preparation of samples. Here, the conjugation of absorbance and fluorescence spectroscopy were used for 5-ASA quantification.

Different concentrations of 5-ASA in PBS were prepared and analysed for absorbance and fluorescence emission in order to allow its quantification. Absorbance measurements were acquired between 280 – 800 nm to assess the absorbance spectrum and the maximum absorbance wavelength (**annex III**). After the initial measurements, the maximum absorbance wavelength was determined as 332 nm (**figure 10**), which is in agreement with literature [42]. Afterwards, a calibration curve was created by applying a

linear regression to the results of absorbance at 332 nm versus concentration – from 0.3 to 0.03 g/L (**figure 11a**). The concentrations of 0.3 g/L and 0.27 g/L were removed for a better adjustment, as these values are outside linearity.

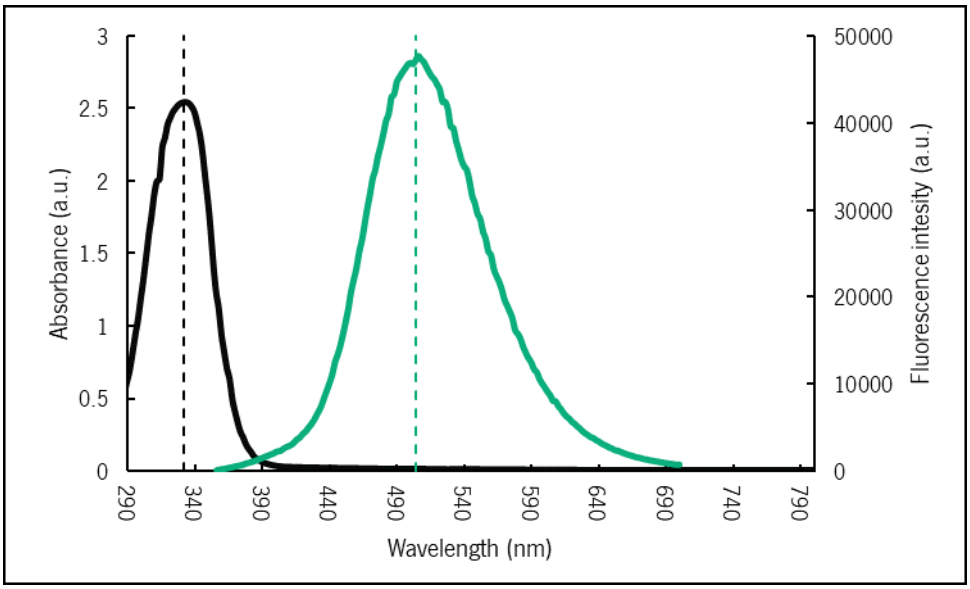

Figure 10 - Absorbance (**black**, primary axis) and emission (**green**, secondary axis) spectra of 5-ASA. Dashed lines indicate the absorbance peak at 332 nm and the fluorescence emission peak at 504 nm.

For the fluorescence emission spectrum, initial optimization studies based on literature allowed to define the excitation wavelength at 300 nm [42]. Similar to the absorbance spectrum, the emission spectrum was acquired over an initial wavelength sweep ranging from 330 nm to 800 nm for the determination of the adequate emission wavelength (**annex III**). Accordingly, the maximum fluorescence emission wavelength obtained was 504 nm, which is very close to previously reported values [42]. The obtained Stokes shift for 5-ASA is 10279 cm^{-1}, suggesting a very different geometry between the emission excited states and the ground states. This also constitutes an advantage when considering detection and quantification by fluorescence spectroscopy, since the difference between the absorption and emission peaks minimize self-quenching. Following the same methodology as in the absorbance spectrum, a linear regression was applied to establish the fluorescence calibration curve (**figure 11b**).

Here, the conjugation of absorbance and fluorescence spectroscopy provides a versatile method for the detection of 5-ASA over a wide range of concentrations – absorbance spectroscopy for higher concentrations and fluorescence spectroscopy for lower concentrations. It is important to note that high

sensitivity of fluorescence spectroscopy allows the detection of very low concentrations of 5-ASA, which is an important feature for the adequate determination of 5-ASA in the cumulative drug release assays. Moreover, both methods are quick and inexpensive, reducing possible errors that could arise from sample preparation and waiting time.

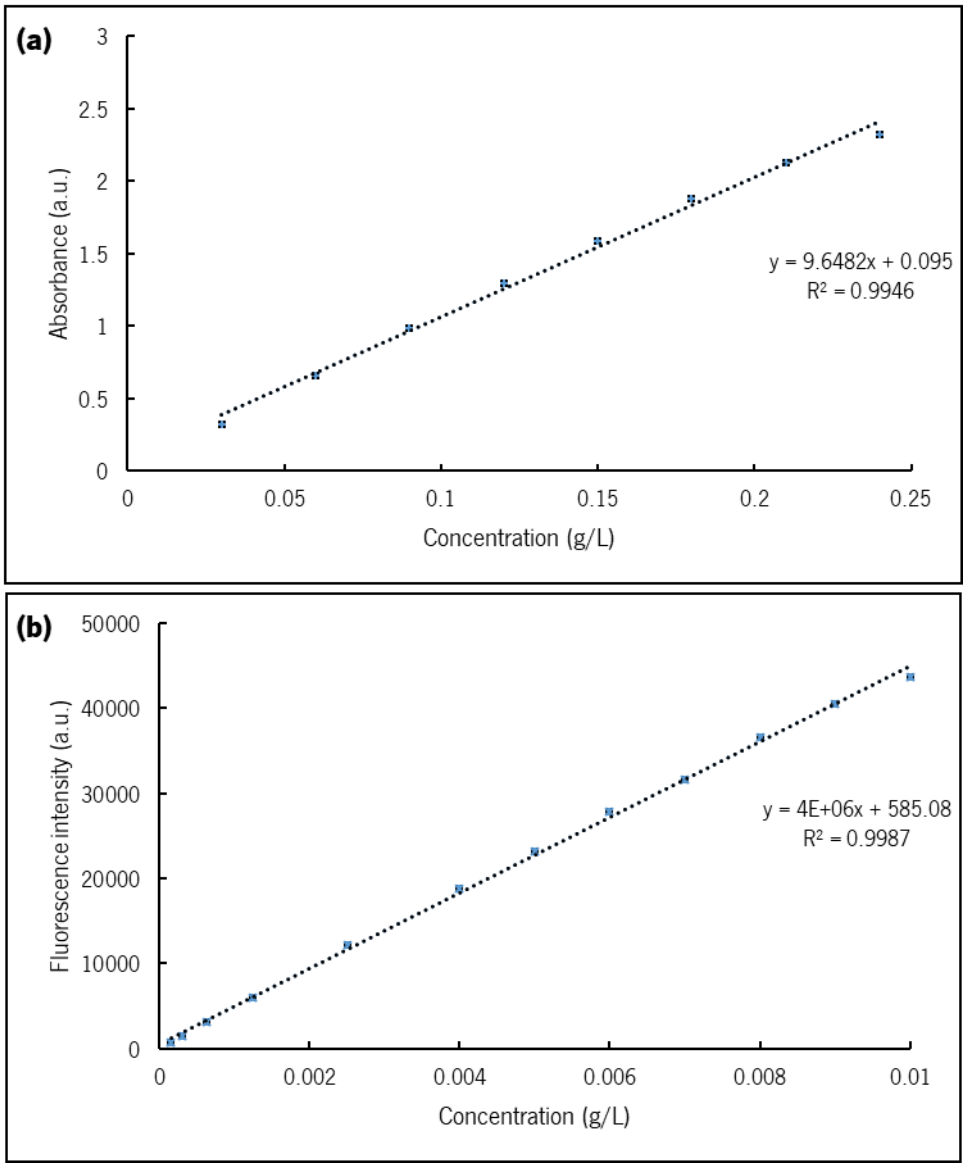

Figure 11 - Absorbance (**a**) and fluorescence (**b**) calibration curves for the quantification of 5-ASA. For each concentration, a total of 9 measurements were performed and plotted with a linear regression.

3.4. Drug entrapment and release

As previously mentioned, this work intends to evaluate the feasibility of using A200 as delivery system for the controlled release of 5-ASA. Previous works already demonstrated a proof-of-concept for the application of A200 as drug delivery platform through the encapsulation of BMPs [114]. Here, the same rationale was used: the entrapment of 5-ASA by inducing the self-assembly of A200 in a solution containing both the drug and the protein polymer. As A200 self-assembles, it was postulated that some amount of 5-ASA would be entrapped within the protein matrix, resulting in 5-ASA loaded particles. To note that a major advantage of the system is the use of mild conditions *i.e.* PBS as dispersing solution and 37 °C for self-assembling.

An initial optimization assay was performed in order to determine an optimal combination of concentrations of A200 and 5-ASA (**table 3**). For this, a combinatorial study involving different concentrations of 5-ASA and different concentrations of A200 was performed to calculate encapsulated concentration (**table 8**) and encapsulation efficiency (**table 9**).

Table 8 - Average encapsulated concentration (in mg/mL) determined from the combinatorial design. A letter code was attributed to the different ELR concentrations, from A to C in decreasing order. A number code was attributed to the different 5-ASA concentrations, from 1 to 5 in decreasing order. [5-ASA]i stands for initial 5-ASA concentration and [A200] stands for A200 concentration.

[5-ASA]i (g/L) / **[A200] (g/L)**	**0.2500 (1)**	**0.1875 (2)**	**0.1250 (3)**	**0.0938 (4)**	**0.0625 (5)**
10 (A)	0.032 ± 0.008	0.016 ± 0.012	0.007 ± 0.007	0.007 ± 0.005	0.007 ± 0.007
5 (B)	0.026 ± 0.008	0.010 ± 0.010	0.007 ± 0.012	0.008 ± 0.005	0.005 ± 0.005
2.5 (C)	0.024 ± 0.013	0.007 ± 0.017	0.005 ± 0.008	0.005 ± 0.004	0.004 ± 0.008

Table 9 – Average encapsulation efficiency (in percentage) determined from the combinatorial design. A letter code was attributed to the different ELR concentrations, from A to C in decreasing order. A number code was attributed to the different 5-ASA concentrations, from 1 to 5 in decreasing order. [5-ASA]i stands for initial 5-ASA concentration and [A200] stands for A200 concentration.

[5-ASA]i (g/L) / **[A200] (g/L)**	**0.2500 (1)**	**0.1875 (2)**	**0.1250 (3)**	**0.0938 (4)**	**0.0625 (5)**
10 (A)	12.77 ± 3.27	8.57 ± 6.63	5.46 ± 5.83	7.32 ± 5.14	10.83 ± 11.92
5 (B)	10.50 ± 3.12	5.17 ± 5.40	5.73 ± 9.37	8.93 ± 5.21	8.38 ± 7.82
2.5 (C)	9.49 ± 5.02	3.79 ± 8.86	3.98 ± 6.67	5.74 ± 4.16	5.99 ± 13.16

According to the results, the combination A1 (10 g/L A200 with 0.25 g/L 5-ASA) resulted in the highest amount of encapsulated drug (0.032 ± 0.008 mg/mL) as well as in the highest encapsulation efficiency (12.8 ± 3.3 %). For the same concentration of 5-ASA, as expected, the combinations with higher concentration of A200 resulted in a higher amount of encapsulated drug (**table 8**). Regarding the EE, results were highly variable with high standard deviation (SD) values. The most consistent formulations, *i.e.*, the combinations with lower SD values, were A1 and B1, showing EE around 12.8 ± 3.27 % and 10.5 ± 3.12 %, respectively. It is also worth noting that, in general, higher standard deviations were observed for combinations with lower concentrations of 5-ASA. Based on the results, the combination A1 was selected for the drug entrapment and release studies. In addition to the average encapsulated concentration and EE, the LC for combination A1 was also determined by application of **equation 4**. Accordingly, the LC was of 0.24 ± 3.2 x 10^{-4} % meaning that, on average, 100 g of A200 particles were loaded with 0.24 g of 5-ASA.

To evaluate if the presence of 5-ASA in the A200 particles could be detected by FTIR analysis, the particles encapsulating the drug, using the combination A1, were collected and analysed by ATR-FTIR (**figure 12**). Analysis of the IR spectrum for unloaded particles and particles loaded with 5-ASA revealed no significant differences. This can be explained by the low content of 5-ASA in the particles, that hinders its detection by ATR-FTIR. As mentioned earlier, the concentration of encapsulated drug was 0.032 g/L (**table 8**) which, experimentally, translates into a total amount of 0.024 mg in the working solution (working volume of 750 µL).

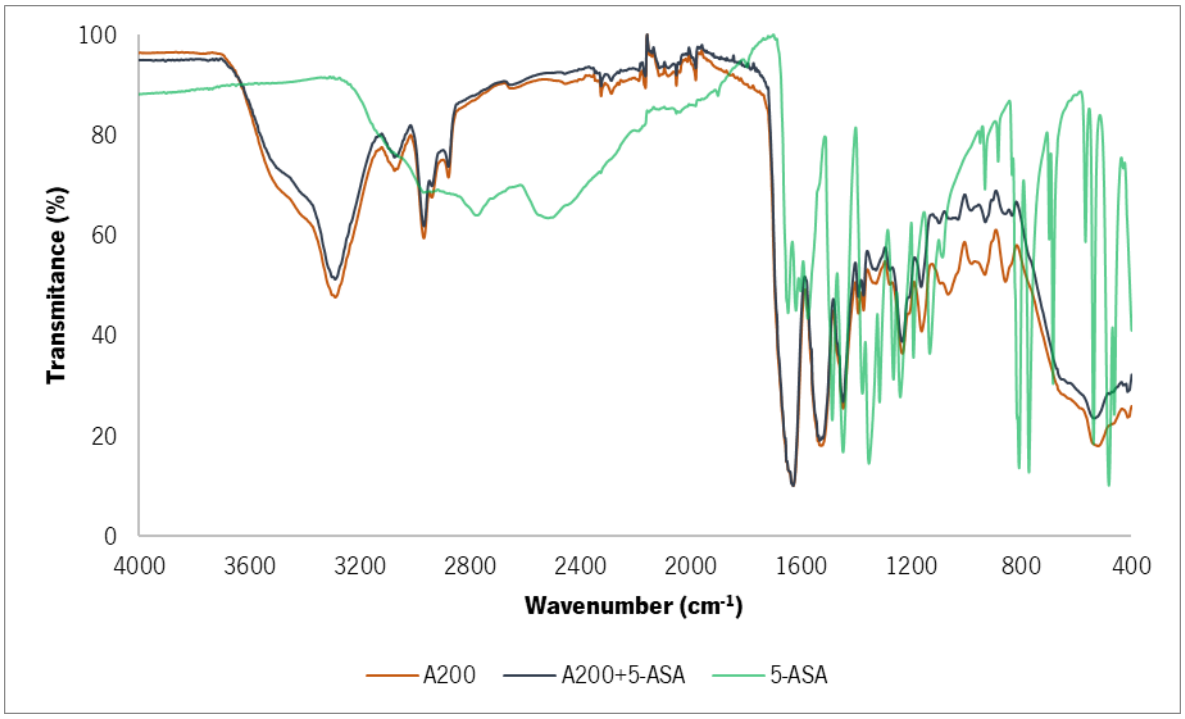

Figure 12 - Infrared spectra of powder 5-ASA (light green), dried A200 (orange) and dried A200 with 5-ASA (dark grey), obtained by AT-FTIR. Transmittance values were normalized.

Previously, it has been demonstrated that A200 was able to encapsulate BMP-2 (≈ 30 kDa; ≈ 30,000 g/mol) and BMP-14 (≈ 27 kDa; ≈ 27,000 g/mol) at high efficiency [114], showing EE values of 94.5 % and 99.2 %, which are significantly larger than those obtained in this study. This is likely explained by the significantly higher molecular weight of BMPs in comparison with 5-ASA (molar mass 153.13 g/mol), although the hydrophobicity also plays an important role [114]. During the self-assembly process of A200, the polypeptide chains aggregate together via a hydrophobic-driven process, forming intertwined mesh-like spherical particles. Due to the size of BMPs, once the self-assembled structures are formed, the release of the growth factors is prevented as these are entrapped within the protein polymer mesh. On the other hand, 5-ASA is a very small molecule and can easily diffuse out of the protein polymer mesh. This hypothesis is further supported by another study involving the encapsulation of dexamethasone phosphate (DMP) (472.4 g/mol) into chemically synthesised poly(VPAVG) particles [116]. The authors demonstrated a loading capacity of about 0.5 %, which is close to the value obtained for 5-ASA, and could help support the hypothesis that the molecular weight and the hydrophobicity of the drug play a major role in its loading into A200 particles.

In the present work, the protein polymer is flanked by three lysine residues at both the N- and C-terminals. It was hypothesized that at pH 7.4 (pH of PBS), 5-ASA would be in its monoanionic form $HASA^-$ and the

lysine residues would be in its monocationic form (**figure 13**). This difference in charge could lead to ionic interactions between 5-ASA and the lysine residues, potentially increasing drug loading. Here, in addition to PBS, water was also considered as solvent. However, since the pH of water is not buffered, the dissolution of 5-ASA can originate a solution with a lower pH, potentially leading to a majority of 5-ASA in its neutral charge state. Moreover, previous experiences demonstrated that the self-assembly of A200 is more efficient in conditions with higher ionic strength as in PBS.

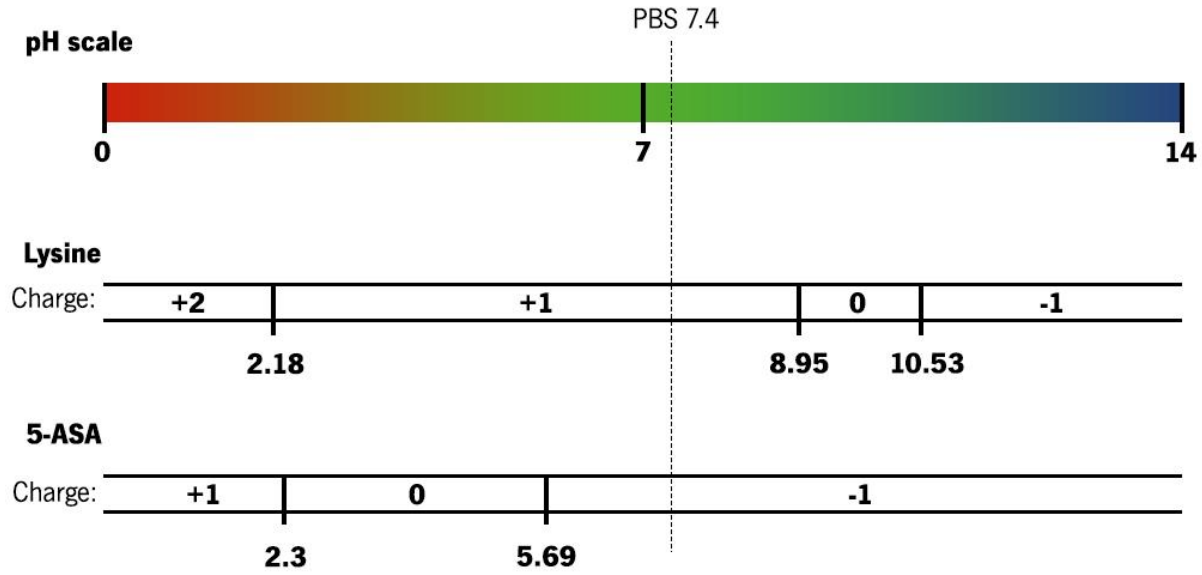

Figure 13 – Predicted charges of lysine and 5-ASA according to their pKa values. The vertical lines and values indicate the pKa values for each molecule and the dashed line represents the pH of PBS.

Compared to other 5-ASA nanoparticulate delivery systems, the EE and LC of A200 nanoparticles are subpar, showing lower values for both parameters (**table 10**). The LC and EE obtained for the A200 nanoparticles are only comparable to mesalazine-PCL bound nanoparticles [91] and Eudragit® S100 nanoparticles [90], respectively. In practical terms, this means that a great amount of the system would need to be administered to meet the effective oral daily dosage of 1.2 g to 2.4 g of 5-ASA. This provides indications that the system is more suitable for the delivery of larger molecules. It is worth noting that most of the systems described in **table 10** offer additional or non-porous barriers, such as surface coatings, inclusion complexes or polymeric nanoparticles, which help to keep the drug inside the particle.

Table 10 – EE and LC values of A200 nanoparticles *vs.* other reported 5-ASA nanoparticle delivery systems. Reports without any mentioned EE and LC values were not included. N/A (not available).

Formulation	**EE(%)**	**LC(%)**	**Reference**
A200 nanoparticles	9.75 ± 1.29	0.24 ± 3.2 x 10^{-4} %	Present work
Surface modified silica nanoparticles	N/A	15.1 ± 6.20 %	73
5-ASA-loaded SiO2 nanoparticles	N/A	13.79 ± 2.50 %	74
SBA-16 silica nanoparticles coated with Eudragit®	N/A	42.1 %	77
Chitosan nanoparticles loaded with hydroxypropyl-β-cyclodextrin/mesalazine inclusion complex	From 75.4 % to 91.4 %	7.5 ± 0.4 %	[131]
Chitosan-carboxymethyl starch nanoparticles	86.7 ± 2.47 % (Polymer concentration of 4 %)	From 10.23 ± 0.50 % to 26.24 ± 0.43 %	81
Dissulfide-linked reduction-sensitive starch nanoparticles	N/A	27.50 % and 30.20 %	84
Eudragit® S100 nanoparticles	From 3.21 ± 0.38 % to 60.51 ± 0.21 %	From 3.35 ± 0.21 % to 21.91 ± 0.56 %	90
Mesalazine-PCL bound nanoparticles	N/A	0.34 ± 0.05 %	91

To characterise the delivery kinetics of the A200/5-ASA based system, drug release assays were performed to calculate the cumulative drug release at time points of 1 h, 2 h, 4 h, 8 h, 24 h and 48 h, following the methodology described in section 2.6. **Figure 14** shows the mean curve for the cumulative drug release of four independent assays, each in triplicate. The cumulative percentage of drug release for each time point is presented in **table 11**.

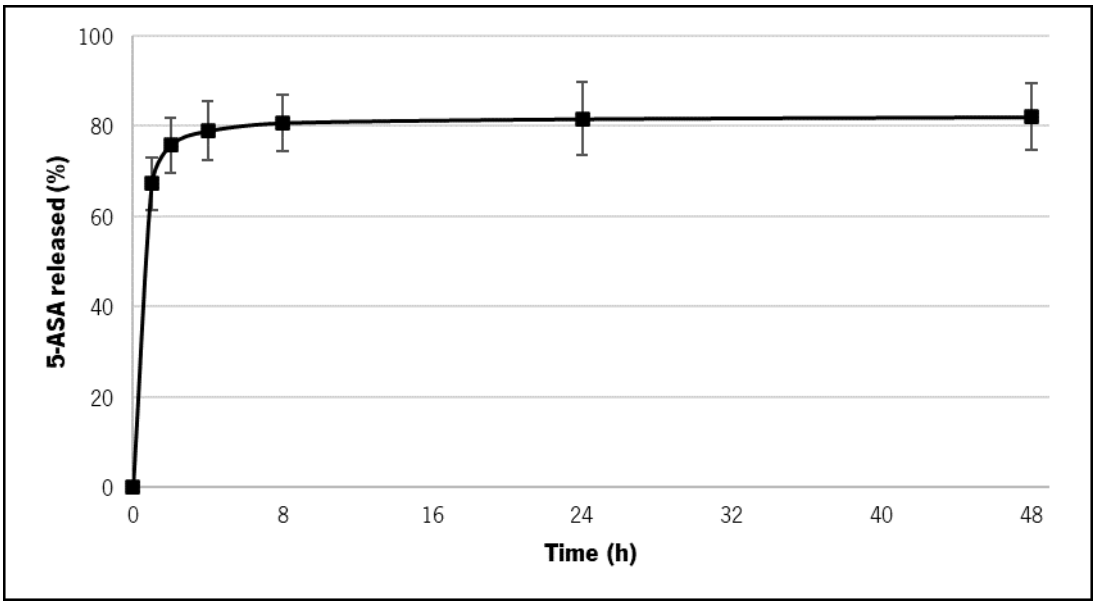

Figure 14 - Mean curve for the cumulative 5-ASA release over time (1 h, 2 h, 4 h, 8 h, 24 h and 48 h) determined from four independent assays, each in triplicate.

Table 11 – Results of the cumulative drug release over time.

Time (h)	**Mean cumulative release (%)**	**SD**
0	0.00	0.00
1	67.28	5.81
2	75.75	6.02
4	78.92	6.63
8	80.68	6.20
24	81.56	8.05
48	82.00	7.43

The drug release profile can be divided in 3 different phases: i) an initial burst occurring during the first hour, ii) a sustained release from 1 h – 8 h, and iii) a minimal steady state release after 8 h. Accordingly, 67.28 ± 5.81 % of the drug is released within the first hour, reaching 80.68 ± 6.20 % after 8 h of the assay. At this point, the release reaches a steady state, and only near 2 % are further released in the following hours up to the end of the experiment (48 h, 82.00 ± 7.43 %). These values are in agreement with those previously observed for poly(VPAVG) encapsulating DMP in which, an initial burst of more than 70 % was observed, followed by a sustained prolonged release over 35 days [116]. Considering a potential oral administration of this system, most of the drug would be released in the stomach (where digestion takes place for 2 h approximatively) and would not reach the intestine.

Nevertheless, one should take in consideration that the experimental procedure used to quantify the amount of loaded 5-ASA may infer some unavoidable errors. Some of the encapsulated 5-ASA may be removed during removal of free drug, thus resulting in an underestimation of the encapsulation efficiency and loading capacity.

3.5. Release kinetics models

The release profile was analysed with DDSolver to determine the release kinetic model showing the best fitting results. A total of eight mathematical models were tested and evaluated according to AdR^2, AIC and MSC parameters. These values are directly correlated with the quality of the fitting for the defined model. In the case of AdR^2 and MSC, the higher the value of the parameter the better appropriateness of the model to fit experimental data [120]. In opposition, lower AIC values are considered as better fit when comparing two models with different number of variables. The AdR^2, compared to R^2, is a more appropriate fitting indicator because it considers the number of variables and overfitting. The AIC is dependent on the magnitude of the data and the number of points [120]. Lastly, the MSC is a modified version of AIC and is independent of the scaling of the data points.

Evaluation of the fitting results for the release kinetic models is represented in **table 12**. Accordingly, five models presented high AdR^2 values (≈ 0.99) namely, from the lowest to the highest, Korsmeyer-Peppas with F0 (0.9878), Korsmeyer-Peppas (0.9902), first-order with Fmax and Tlag (0.9967), first-order with Fmax (0.9974), and Korsmeyer-Peppas with Tlag (0.9992). From these, Korsmeyer-Peppas with Tlag and First-order with Fmax present the lowest AIC values and the highest MSC values.

Table 12 – Drug release kinetic models and respective fitting parameters AdR^2, AIC and MSC for the cumulative release assay. In all equations, F stands for the fraction (%) of drug released at time t. k0 is the zero-order release constant; k1 is the first-order release constant; Fmax is the maximum fraction of drug released at infinite; Tlag is the lag time preceding drug release; kH is the release constant for the Higuchi model; kHC is the release constant for the Hixton-Crowell model; kKP is the release constant for the Korsmeyer-Peppas model; n is the diffusional exponent; F0 is the fraction for the initial burst release.

Model	Equation	AdR^2	AIC	MSC
Zero-order	$F = k_0 \cdot t$	-2.6586	71.15	-3.37
First-order	$F = 100 \cdot (1 - e^{-k_1 \cdot t})$	0.7218	53.11	-0.79
First order with Fmax	$F = F_{max} \cdot (1 - e^{-k_1 \cdot t})$	0.9974	21.18	3.77
First order with Fmax and Tlag	$F = F_{max} \cdot [1 - e^{-k_1 \cdot (t - Tlag)}]$	0.9967	23.18	3.49
Higuchi	$F = k_H \cdot t^{0.5}$	-0.9908	66.89	-2.76
Hixton-Crowell	$F = 100 \cdot [1 - (1 - k_{HC} \cdot t)^3]$	-0.9908	66.89	-2.76
Korsmeyer-Peppas	$F = k_{KP} \cdot t^n$	0.9902	30.38	2.46
Korsmeyer-Peppas with F0	$F = F0 + k_{KP} \cdot t^n$	0.9878	32.38	2.17
Korsmeyer-Peppas with Tlag	$F = k_{KP} \cdot (t - T_{lag})^n$	0.9992	12.94	4.95

Based on the fitting values and according to the AdR^2 values, the best model to characterize the release of 5-ASA from the A200 particles would be variations of the Korsmeyer-Peppas model (Korsmeyer-Peppas or Korsmeyer-Peppas with Tlag) or of first-order release (first-order with Fmax and first-order with Fmax and Tlag). Although the fitting parameters AdR^2, AIC and MSC are helpful in selecting the most appropriate mathematical model, it should always be complemented with a critical analysis of the system and the most plausible assumption of the drug release mechanism, which is dependent on its nature [120]. There are two major differences between the mechanistic assumptions for the first-order and the Korsmeyer-Peppas models. The first-order release model is entirely based on Fick's law of diffusion and assumes the system is a drug reservoir covered with a barrier membrane that ultimately controls the diffusion rate. It also assumes that the drug concentration inside this barrier is below the drug solubility [132]. Given that this membrane does not dissolve or swell, if perfect sink conditions are provided throughout the release

process and if the drug permeability through the barrier is constant, diffusion is the only process that controls the release rate and first-order kinetics predicts the release rate.

For the Korsmeyer-Peppas models, in addition to Fick's law of diffusion, polymer swelling also plays a relevant role in the release rate. One major consequence of polymer swelling in the release rate is the generation of a longer diffusion path and consequent decreasing drug concentration gradients, which can decrease the release rate [132]. This occurs because the polymer swells from the outside in, from a less mobile state to a mobile state.

Since the A200 self-assembled structures are a polypeptidic system and do not present a coating barrier, the most logical choice between first-order or Korsmeyer-Peppas model variations would be the latter. Moreover, other works with this system have shown a rapid swelling, with a water uptake of 261.9 ± 41 % in the first 30 min [114], which is a key proposition of the Korsmeyer-Peppas model. Regarding this model, there are two variations of the original equation: one used to describe a late onset of the release rate (Tlag) and the other used to describe an initial burst drug release (F_0). In this work, the variation with Tlag, presents the best AdR^2 and MSC values. However, in this model, the obtained value of Tlag was of 0.99 which overestimates the fitting as a consequence of the experimental data. It is safe to assume that the drug is continuously released before the first measurement at the first hour. Hence, the hypothetical late onset associated with this model cannot be confirmed from these results alone and this model should be disregarded. For this reason, the standard Korsmeyer-Peppas model was considered as the most appropriate model to describe the release mechanism of the A200 system. **Figure 15** presents the curves for both models and the model equations for standard Korsmeyer-Peppas and Korspeyer-Peppas with Tlag are represented as **equations 6** and **7**, respectively.

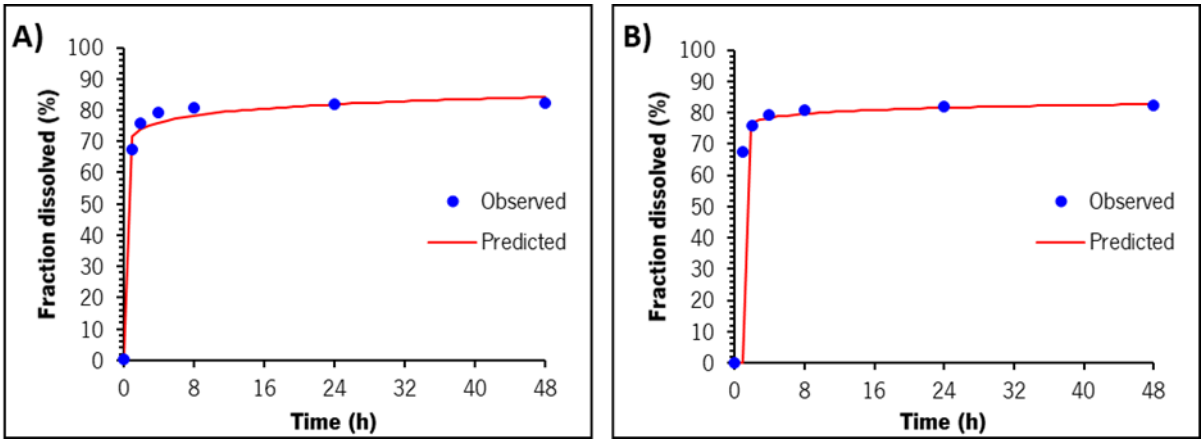

Figure 15 - Drug release kinetics curve fitted with the A) Korsmeyer-Peppas and B) Korsmeyer-Peppas with Tlag, using DDSolver.

Eq. 6 $$F = 71.891 \cdot t^{0.041}$$

Eq. 7 $$F = 76.692 \cdot (t - 0.999)^{0.02}$$

Ultimately, while Korsmeyer-Peppas with Tlag provides a better mathematical fit for the release kinetics, the empirical basis of the standard Korsmeyer-Peppas model better describes the physical process behind the release of 5-ASA from the A200 nanoparticles. In the present work, the fit for the Korsmeyer-Peppas with Tlag is conditioned by the experimental data and additional time points before the first hour would be needed to confirm if the late onset of the release rate occurs.

3.6. Particle morphology

SEM was used to determine the morphology and size of loaded and unloaded particles (**figure 16**), demonstrating the formation of spherical nanoparticles with mean diameters of 44.09 ± 7.25 nm and 45.81 ± 9.62 nm for the unloaded and 5-ASA particles, respectively. These results contrast with those obtained by DLS. However, one must consider that the particles for SEM are fully dried in opposition to the hydrated samples used in DLS. These differences in size between dried and hydrated particles also provide indications for the high-water content in the self-assembled A200 particles.

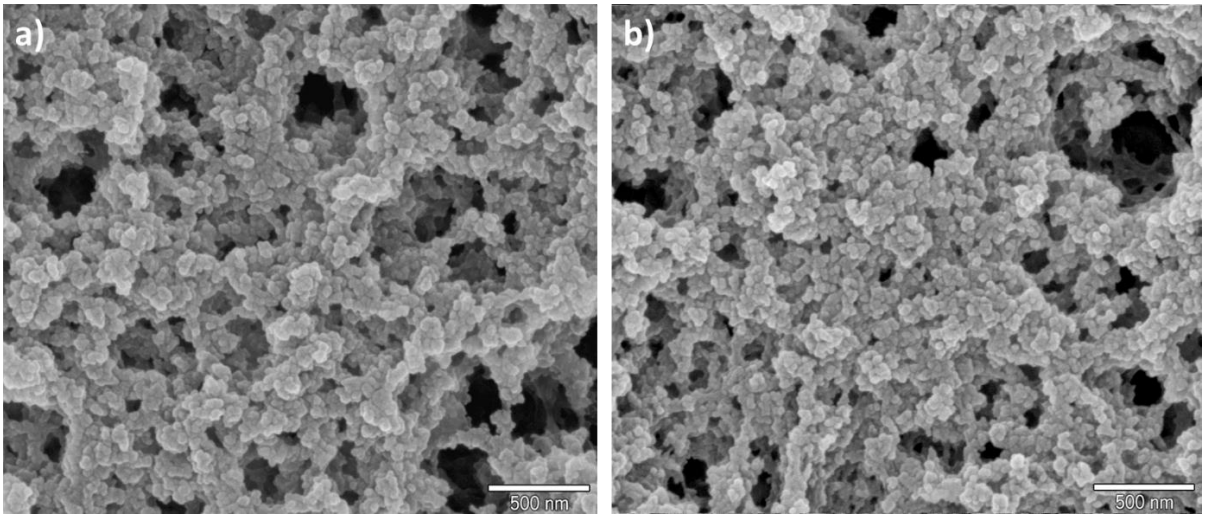

Figure 16 - SEM micrographs for unloaded A200 particles (left) and 5-ASA loaded particles (right).

4. Conclusions and future perspectives

The main objective of this thesis was to evaluate the feasibility of using ELR as a platform for the oral delivery of 5-ASA, targeting the development of novel therapies for IBD. Additionally, it also aimed at contributing to expand the knowledge on ELR-based delivery systems by assessing its potential for the encapsulation of small drugs.

Here, an ELR consisting of 200 repetitions of the pentamer VPAVG was used as delivery system for 5-ASA. Purification of A200 was easily achieved by exploring the phase transition behaviour of ELR, avoiding the need of cumbersome chromatographic methods and resulting in highly pure protein polymer fractions with high recovery rate. In the characterization of a drug delivery system, there is the need to implement methodologies that allow for a proper quantification of the loaded/released drug. Absorbance and fluorescence spectroscopy proved to be a viable combination of methods for the quantification of 5-ASA with the advantages of reduced cost and time of operation. Fluorescence spectroscopy also provides a very sensitive methodology, allowing for the quantification of small concentrations.

ELR, and specifically A200, are highly interesting biomolecules for the development of drug delivery systems due to the associated biocompatibility and spontaneous self-assembly behaviour in mild conditions (*i.e.* PBS and 37 °C). However, for the specific case considered in this thesis, the system demonstrated to present limitations deriving from the low encapsulation efficiency and loading capacity, and fast release of 5-ASA. In fact, the low loading capacity of the system would require a great amount of encapsulated drug to meet the daily oral dosage between 1.2 g and 2.4 g. Moreover, the release kinetics are associated with an initial burst, with almost all the loaded drug being released within the first eight hours, and great part in the first two hours. This is not ideal for oral delivery in therapies targeting the intestine, as most of the drug would be released in the stomach (where digestion takes place for 2 h approximatively) and would not reach the target. Despite these results, the characterization of the release mechanism provides a valuable contribution to the understanding of A200 as a potential drug delivery platform. The fit to Korsmeyer-Peppas kinetic model suggests a mixed diffusion-swelling based release. The system swelling can be very useful for the sustained release of pharmaceuticals since the concentration gradient, which is the main force driving diffusion, is smaller and with a longer pathway. The same release system is found in hydroxypropyl methylcellulose, a common excipient in oral pharmaceuticals. This opens the door to explore the system as a matrix in combination with other materials.

An interesting strategy to overcome the limitations associated with the fast release and low loading performance would be by cross-linking 5-ASA with the lysine residues of A200 by an azo-bond. Azo-bonds are typically used in 5-ASA prodrugs since they are known to be reduced by colonic bacteria. This strategy would improve the loading efficiency and would slow the release up to the intestine. Alternatively, or in combination, the use of pH-dependent excipients like Eudragit® could possibly delay release and provide a colon-targeted delivery.

Finally, an important consideration that can be extrapolated from this work and should be considered for future research with A200 as delivery system is the relation between the loading efficiency and the size of the drug to be loaded. A comparison between this work and literature suggests a positive correlation between the molecular weight of the drug with the encapsulation efficiency, although properties like hydrophobicity should be also considered. This could indicate that A200 is more adequate for the delivery of larger molecules. Hence, an interesting study would be to characterize the loading and release profile of molecules with different sizes and hydrophobicity in A200.

5. References

1. Zhang, Y.-Z. & Li, Y.-Y. Inflammatory bowel disease: Pathogenesis. *World J. Gastroenterol.* **20**, 91–99 (2014).

2. Harmsen, W. S., Tremaine, W. J. & Loftus, E. V. Incidence of inflammatory bowel disease by race and ethnicity in a population-based inception cohort from 1970 through 2010. *Therap. Adv. Gastroenterol.* **1**, 1–8 (2019).

3. Burisch, J. & Munkholm, P. The epidemiology of inflammatory bowel disease. *Scand. J. Gastroenterol.* **50**, 942–951 (2015).

4. Ng, S. C., Shi, H. Y., Hamidi, N., Underwood, F. E., *et al.* Worldwide incidence and prevalence of inflammatory bowel disease in the 21st century: a systematic review of population-based studies. *Lancet* **390**, 2769–2778 (2017).

5. Schreiber, S. The complicated path to true causes of disease: role of nuclear factor κB in inflammatory bowel disease. *Gut* **54**, 444 LP – 445 (2005).

6. Hansen, J. J. Immune Responses to Intestinal Microbes in Inflammatory Bowel Diseases. *Curr. Allergy Asthma Rep.* **15**, 61 (2015).

7. Evans-Marin, H. L. & Cong, Y. Microbiota Regulation of Inflammatory Bowel Disease. *Inflamm. Allergy - Drug Targets* **13**, 65–73 (2014).

8. Lee, H.-S., Choe, J., Kim, S.-O., Lee, S.-H., *et al.* Overall and Cause-specific Mortality in Korean Patients with Inflammatory Bowel Disease: A Hospital-based Cohort Study. *J. Gastroenterol. Hepatol.* **32**, 782–788 (2017).

9. Kassam, Z., Belga, S., Roifman, I., Hirota, S., *et al.* Inflammatory Bowel Disease Cause-specific Mortality: A Primer for Clinicians. *Inflamm. Bowel Dis.* **20**, 2483–2492 (2014).

10. Witte, J., Shivananda, S., Lennard-Jones, J. E., Beltrami, M., *et al.* Disease Outcome in Inflammatory Bowel Disease: Mortality, Morbidity and Therapeutic Management of a 796-Person Inception Cohort in the European Collaborative Study on Inflammatory Bowel Disease (EC-IBD). *Scand. J. Gastroenterol.* **35**, 1272–1277 (2000).

11. Alatab, S., Sepanlou, S. G., Ikuta, K., Vahedi, H., *et al.* The global, regional, and national burden of inflammatory bowel disease in 195 countries and territories, 1990–2017: a systematic analysis

for the Global Burden of Disease Study 2017. *Lancet Gastroenterol. Hepatol.* **5**, 17–30 (2020).

12. Sexton, K. A., Walker, J. R., Targownik, L. E., Graff, L. A., *et al.* The Inflammatory Bowel Disease Symptom Inventory: A Patient-report Scale for Research and Clinical Application. *Inflamm. Bowel Dis.* **25**, 1277–1290 (2019).

13. Sairenji, T., Collins, K. L. & Evans, D. V. An Update on Inflammatory Bowel Disease. *Prim. Care Clin. Off. Pract.* **44**, 673–692 (2017).

14. Addolorato, G., Capristo, E., Stefanini, G. F. & Gasbarrini, G. Inflammatory Bowel Disease: A Study of the Association between Anxiety and Depression, Physical Morbidity, and Nutritional Status. *Scand. J. Gastroenterol.* **32**, 1013–1021 (1997).

15. Reigada, L. C., Bruzzese, J.-M., Benkov, K. J., Levy, J., *et al.* Illness-specific anxiety: Implications for functioning and utilization of medical services in adolescents with inflammatory bowel disease. *J. Spec. Pedriatric Nurs.* **16**, 207–215 (2011).

16. Xu, X., Liu, C.-Q., Feng, B.-S. & Liu, Z.-J. Dysregulation of mucosal immune response in pathogenesis of inflammatory bowel disease. *World J. Gastroenterol.* **20**, 3255–3264 (2014).

17. Di Paolo, M. C., Paoluzi, O. A., Pica, R., Iacopini, F., *et al.* Sulphasalazine and 5-aminosalicylic acid in long-term treatment of ulcerative colitis: report on tolerance and side-effecs. *Dig. Liver Dis.* **33**, 563–569 (2001).

18. Rutgeerts, P. J. Review article: the limitations of corticosteroid therapy in Crohn's disease. *Aliment. Pharmacol. Ther.* **15**, 1515–1525 (2001).

19. Shivaji, U. N., Sharratt, C. L., Thomas, T., Smith, S. C. L., *et al.* Review article: managing the adverse events caused by anti-TNF therapy in inflammatory bowel disease. *Aliment. Pharmacol. Ther.* **49**, 664–680 (2019).

20. Ei, B., Ch, S., Ah, S. & Am, G. Traditional corticosteroids for induction of remission in Crohn's disease (Review). *Chochrane Database Syst. Rev.* (2008) doi:10.1002/14651858.CD006792.pub2.

21. Gionchetti, P., Rizzello, F., Annese, V., Armuzzi, A., *et al.* Use of corticosteroids and immunosuppressive drugs in inflammatory bowel disease: Clinical practice guidelines of the Italian Group for the Study of Inflammatory Bowel Disease. *Dig. Liver Dis.* **49**, 604–617 (2017).

22. De Cassan, C., Fiorino, G. & Danese, S. Second-Generation Corticosteroids for the Treatment of Crohn's Disease and Ulcerative Colitis: More Effective and Less Side Effects? *Dig. Dis.* **30**, 368–375 (2012).

23. Saibeni, S., Bollani, S., Losco, A., Michielan, A., *et al.* The use of methotrexate for treatment of inflammatory bowel disease in clinical practice. *Dig. Liver Dis.* **44**, 123–127 (2012).

24. Nielsen, O. H., Vainer, B. & Rask-Madsen, J. Review article: the treatment of in inflammatory bowel disease with 6-mercaptopurine or azathioprine. *Aliment. Pharmacol. Ther.* **15**, 1699–1708 (2001).

25. Khan, K. J., Dubinsky, M. C., Ford, A. C., Ullman, T. A., *et al.* Efficacy of Immunosuppressive Therapy for Inflammatory Bowel Disease: A Systematic Review and Meta-Analysis. *Am. J. Gastroenterol.* **106**, 630–642 (2011).

26. Profile, D. Azathioprine in inflammatory bowel disease: improved molecular insights and resulting clinical implications. *Expert Rev. Gastroenterol. Hepatol.* 23–34 (2008).

27. Corica, D. & Romano, C. Biological Therapy in Pediatric Inflammatory Bowel Disease: A Systematic Review. *J. Clin. Gastroenterol.* **51**, 100–110 (2017).

28. Cholapranee, A., Hazlewood, G. S., Kaplan, G. G., Peyrin-Biroulet, L., *et al.* Systematic review with meta-analysis: Comparative efficacy of biologics for induction and maintenance of mucosal healing in Crohn's disease and ulcerative colitis controlled trials. *Aliment. Pharmacol. Ther.* **45**, 1291–1302 (2017).

29. Moss, A. C. Mechanism of Action and Pharmacokinetics of Biologics. in *Treatment of Inflammatory Bowel Disease With Biologics* (eds. Cheifetz, A. & Feuerstein, J.) 1–11 (Springer, Cham, 2017). doi:https://doi.org/10.1007/978-3-319-60276-9_1.

30. Hindryckx, P., Novak, G., Bonovas, S., Peyrin-Biroulet, L., *et al.* Infection Risk With Biologic Therapy in Patients With Inflammatory Bowel Disease. *Clin. Pharmacol. Ther.* **102**, 633–641 (2017).

31. Sartini, A., Scaioli, E., Liverani, E., Bellanova, M., *et al.* Retention Rate, Persistence and Safety of Adalimumab in Inflammatory Bowel Disease: A Real-Life, 9-Year, Single-Center Experience in Italy. *Dig. Dis. Sci.* **64**, 863–874 (2019).

32. Williams, C., Panaccione, R., Ghosh, S. & Rioux, K. Optimizing clinical use of mesalazine (5-

aminosalicylic acid) in inflammatory bowel disease. *Therap. Adv. Gastroenterol.* 237–248 (2015) doi:10.1177/1756283X11405250.

33. Desreumaux, P. & Ghosh, S. Review article: mode of action and delivery of 5-aminosalicylic acid – new evidence. *Aliment. Pharmacol. Ther.* **24**, 2–9 (2006).

34. Ma, C., Ascoytia, C., Mccarrier, K. P., Martin, M., *et al.* Physicians' Perspectives on Cost, Safety, and Perceived Efficacy Determine Aminosalicylate Use in Crohn's Disease. *Dig. Dis. Sci.* **63**, 2555–2563 (2018).

35. Results, A. T. & Svartz, N. Salazopyrin, a new sulfanilamide preparation. *Acta Med. Scand.* **110**, 577–598 (1942).

36. Hauso, Ø., Martinsen, T. C. & Waldum, H. 5-Aminosalicylic acid, a specific drug for ulcerative colitis. *Scand. J. Gastroenterol.* **50**, 933–941 (2015).

37. Roldo, M., Barbu, E., Brown, J. F., Laight, D. W., *et al.* Azo compounds in colon-specific drug delivery. *Expert Opin. Drug Deliv.* **4**, 547–560 (2007).

38. Jr, E. V. L., Ane, S. V. K. & Bjorkma, D. N. Systematic review: short-term adverse effects of 5-aminosalicylic acid agents in the treatment of ulcerative colitis. *Aliment. Pharmacol. Ther.* **19**, 179–189 (2004).

39. Ford, A. C., Achkar, J.-P., Khan, K. J., Kane, S. V, *et al.* Efficacy of 5-Aminosalicylates in Ulcerative Colitis: Systematic Review and Meta-Analysis. *Am. J. Gastroenterol.* **106**, 601–616 (2011).

40. Singh, S., Feuerstein, J. D., Binion, D. G. & Tremaine, W. J. AGA Technical Review on the Management of Mild-to-Moderate Ulcerative Colitis. *Gastroenterology* **156**, 769-808.e29 (2019).

41. French, D. L. & Mauger, J. W. Evaluation of the Physicochemical Properties and Dissolution Characteristics of Mesalamine: Relevance of Controlled Intestinal Drug Delivery. *Pharm. Res.* **10**, 1285–1290 (1993).

42. Pozdnyakov, I. P., Pigliucci, A., Tkachenko, N., Plyusnin, V. F., *et al.* The photophysics of salicylic acid derivatives in aqueous solution. *J. Phys. Org. Chem.* **22**, 449–454 (2009).

43. Berends, S. E., Strik, A. S., Löwenberg, M., D'Haens, G. R., *et al.* Clinical Pharmacokinetic and Pharmacodynamic Considerations in the Treatment of Ulcerative Colitis. *Clin. Pharmacokinet.* **58**, 15–37 (2019).

44. Moyer, M. S. 5-Aminosalicylate Therapy. in *Pediatric Inflammatory Bowel Disease* (eds. Mamula, P., Markowitz, J. E. & Baldassano, R. N.) 317–328 (Springer US, 2008). doi:10.1007/978-0-387-73481-1_24.

45. Zhou, S. Y., Fleisher, D., Pao, L. H., Li, C., *et al.* Intestinal Metabolism and Transport of 5-aminosalicylate. *Drug Metab. Dispos.* **27**, 479–485 (1999).

46. Ham, M. & Moss, A. C. Mesalamine in the treatment and maintenance of remission of ulcerative colitis. *Expert Rev. Clin. Pharmacol.* **5**, 113–123 (2012).

47. Lim, W., Wang, Y., MacDonald, J. & Hanauer, S. Aminosalicylates for induction of remission or response in Crohn's disease (Review). *Cochrane Database Syst. Rev.* Art. No.: CD008870 (2016) doi:10.1002/14651858.CD008870.pub2.www.cochranelibrary.com.

48. Gjuladin-Hellon, T., Gordon, M., Iheozor-Ejiofor, Z. & Akonbeng, A. Oral 5-aminosalicylic acid for maintenance of surgically-induced remission in Crohn's disease (Review). *Cochrane Database Syst. Rev.* Art. No.: CD008414 (2019) doi:10.1002/14651858.CD008414.pub3.Copyright.

49. Matthis, A. L., Zhang, B., Denson, L. A., Yacyshyn, B. R., *et al.* Importance of the Evaluation of N-Acetyltransferase Enzyme Activity Prior to 5-Aminosalicylic Acid Medication for Ulcerative Colitis. *Inflamm. Bowel Dis.* **22**, 1793–1802 (2016).

50. Hussain, F. N., Ajjan, R. A. & Riley, S. A. Dose loading with delayed-release mesalazine: a study of tissue drug concentrations and standard pharmacokinetic parameters. *Br. J. Clin. Pharmacol.* **49**, 323–330 (2000).

51. Stolfi, C., De Simone, V., Pallone, F. & Monteleone, G. Mechanisms of Action of Non-Steroidal Anti-Inflammatory Drugs (NSAIDs) and Mesalazine in the Chemoprevention of Colorectal Cancer. *Int. J. Mol. Sci.* **14**, 17972–17985 (2013).

52. Allgayer, H. Review article: mechanisms of action of mesalazine in preventing colorectal carcinoma in inflammatory bowel disease. *Aliment. Pharmacol. Ther.* **18**, 10–14 (2003).

53. Ning, L., Lou, X., Zhang, F. & Xu, G. Nuclear Receptors in the Pathogenesis and Management of Inflammatory Bowel Disease. *Mediators Inflamm.* **2019**, (2019).

54. Lawrence, T. The Nuclear Factor NF-κB Pathway In Inflammation. *Cold Spring Harb. Perspect. Biol.* **1**, a001651 (2009).

55. Sokollik, C., Fournier, N., Rizzuti, D., Braegger, C. P., *et al.* The Use of 5-Aminosalicylic Acid in Children and Adolescents With Inflammatory Bowel Disease. *J. Clin. Gastroenterol.* **51**, e87–e91 (2018).

56. Marshall, J., Thabane, M., Steinhart, A., Newman, J., *et al.* Rectal 5-aminosalicylic acid for induction of remission in ulcerative colitis (Review). *Cochrane Database Syst. Rev.* Art. No.: CD004115 (2010) doi:10.1002/14651858.CD004115.pub2.

57. Peyrin-Biroulet, L. & Lémann, M. Review article: remission rates achievable by current therapies for inflammatory bowel disease. *Aliment. Pharmacol. Ther.* **33**, 870–879 (2011).

58. Rousseaux, C., El-Jamal, N., Fumery, M., Dubuquoy, C., *et al.* The 5-aminosalicylic acid antineoplastic effect in the intestine is mediated by PPARγ. *Carginogenesis* **34**, 2580–2586 (2013).

59. Kim, Y.-H., Kim, M. H., Kim, B. J., Kim, J. J., *et al.* Inhibition of cell proliferation and invasion in a human colon cancer cell line by 5-aminosalicylic acid. *Dig. Liver Dis.* **41**, 328–337 (2009).

60. Qiu, X., Ma, J., Wang, K. & Zhang, H. Chemopreventive effects of 5-aminosalicylic acid on inflammatory bowel disease-associated colorectal cancer and dysplasia: a systematic review with meta-analysis. *Oncotarget* **8**, 1031–1045 (2017).

61. Bajpai, M., Seril, D. N., Van Gurp, J., Geng, X., *et al.* Effect of Long-Term Mesalamine Therapy on Cancer-Associated Gene Expression in Colonic Mucosa of Patients with Ulcerative Colitis. *Dig. Dis. Sci.* **64**, 740–750 (2019).

62. Hua, S., Marks, E., Schneider, J. J. & Keely, S. Advances in oral nano-delivery systems for colon targeted drug delivery in inflammatory bowel disease: Selective targeting to diseased versus healthy tissue. *Nanomedicine Nanotechnology, Biol. Med.* **11**, 1117–1132 (2015).

63. Hunt, R. H., Camilleri, M., Crowe, S. E., El-Omar, E. M., *et al.* The stomach in health and disease. *Gut* **64**, 1650–1668 (2015).

64. Nugent, S. G. & Kumar, D. Intestinal luminal pH in inflammatory bowel disease: possible determinants and implications for therapy with aminosalicylates and other drugs. *Gut* **48**, 571–577 (2001).

65. Nugent, S. G., Kumar, D., Rampton, D. S. & Evans, D. F. Intestinal luminal pH in inflammatory

bowel disease: possible determinants and implications for therapy with aminosalicylates and other drugs. *Gut* **48**, 571–577 (2001).

66. Malayandi, R., Kondamudi, P. K., Ruby, P. K. & Aggarwal, D. Biopharmaceutical considerations and characterizations in development of colon targeted dosage forms for inflammatory bowel disease. *Drug Deliv. Transl. Res.* **4**, 187–202 (2014).

67. Sinha, V. R. & Kumria, R. Polysaccharides in colon-specific drug delivery. *Int. J. Pharm.* **224**, 19–38 (2001).

68. Thakral, S., Thakral, N. K. & Majumdar, D. K. Eudragit: a technology evaluation. *Expert Opin. Drug Deliv.* **10**, 131–149 (2013).

69. Seibold, F., Fournier, N., Beglinger, C., Mottet, C., *et al.* Topical therapy is underused in patients with ulcerative colitis. *J. Crohn's Colitis* **8**, 56–63 (2014).

70. Harris, M. S. & Lichtenstein, G. R. Review article: delivery and efficacy of topical 5-aminosalicylic acid (mesalazine) therapy in the treatment of ulcerative colitis. *Aliment. Pharmacol. Ther.* **33**, 996–1009 (2011).

71. Collnot, E.-M., Ali, H. & Lehr, C.-M. Nano- and microparticulate drug carriers for targeting of the inflamed intestinal mucosa. *J. Control. Release* **161**, 235–246 (2012).

72. Lamprecht, A., Yamamoto, H., Takeuchi, H. & Kawashima, Y. Nanoparticles Enhance Therapeutic Efficiency by Selectively Increased Local Drug Dose in Experimental Colitis in Rats. *J. Pharmacol. Exp. Ther.* **315**, 196–202 (2005).

73. Moulari, B., Pertuit, D., Pellequer, Y. & Lamprecht, A. The targeting of surface modified silica nanoparticles to inflamed tissue in experimental colitis. *Biomaterials* **29**, 4554–4560 (2008).

74. Tang, H., Xiang, D., Wang, F., Mao, J., *et al.* 5-ASA-loaded SiO2 nanoparticles-a novel drug delivery system targeting therapy on ulcerative colitis in mice. *Mol. Med. Rep.* **15**, 1117–1122 (2017).

75. Teruel, A. H., Pérez-Esteve, É., González-Álvarez, I., González-Álvarez, M., *et al.* Double Drug Delivery Using Capped Mesoporous Silica Microparticles for the Effective Treatment of Inflammatory Bowel Disease. *Mol. Pharm.* **16**, 2418–2429 (2019).

76. Zhang, H., Shahbazi, M.-A., Mäkilä, E. M., da Silva, T. H., *et al.* Diatom silica microparticles for sustained release and permeation enhancement following oral delivery of prednisone and

mesalamine. *Biomaterials* **34**, 9210–9219 (2013).

77. Trendafilova, I., Szegedi, Á., Yoncheva, K., Shestakova, P., *et al.* A pH dependent delivery of mesalazine from polymer coated and drug-loaded SBA-16 systems. *Eur. J. Pharm. Sci.* **81**, 75–81 (2016).

78. Mladenovska, K., Raicki, R. S., Janevik, E. I., Ristoski, T., *et al.* Colon-specific delivery of 5-aminosalicylic acid from chitosan-Ca-alginate microparticles. *Int. J. Pharm.* **342**, 124–136 (2007).

79. Duan, H., Lü, S., Gao, C., Bai, X., *et al.* Mucoadhesive microparticulates based on polysaccharide for target dual drug delivery of 5-aminosalicylic acid and curcumin to inflamed colon. *Colloids Surfaces B Biointerfaces* **145**, 510–519 (2016).

80. Tang, P., Sun, Q., Zhao, L., Pu, H., *et al.* Mesalazine/hydroxypropyl-β-cyclodextrin/chitosan nanoparticles with sustained release and enhanced anti-inflammation activity. *Carbohydr. Polym.* **198**, 418–425 (2018).

81. Saboktakin, M. R., Tabatabaie, R. M., Maharramov, A. & Ramazanov, M. A. Synthesis and in vitro evaluation of carboxymethyl starch–chitosan nanoparticles as drug delivery system to the colon. *Int. J. Biol. Macromol.* **48**, 381–385 (2011).

82. Palma, E., Costa, N., Molinaro, R., Francardi, M., *et al.* Improvement of the therapeutic treatment of inflammatory bowel diseases following rectal administration of mesalazine-loaded chitosan microparticles vs Asamax®. *Carbohydr. Polym.* **212**, 430–438 (2019).

83. Walz, M., Hagemann, D., Trentzsch, M., Weber, A., *et al.* Degradation studies of modified inulin as potential encapsulation material for colon targeting and release of mesalamine. *Carbohydr. Polym.* **199**, 102–108 (2018).

84. Yang, J., Huang, Y., Gao, C., Liu, M., *et al.* Fabrication and evaluation of the novel reduction-sensitive starch nanoparticles for controlled drug release. *Colloids Surfaces B Biointerfaces* **115**, 368–376 (2014).

85. Chen, J., Li, X., Chen, L. & Xie, F. Starch film-coated microparticles for oral colon-specific drug delivery. *Carbohydr. Polym.* **191**, 242–254 (2018).

86. Singh, V., Joshi, S. & Malviya, T. Carboxymethyl cellulose-rosin gum hybrid nanoparticles: An

efficient drug carrier. *Int. J. Biol. Macromol.* **112**, 390–398 (2018).

87. Kumar, S. & Negi, Y. S. Nanoparticles Synthesis from Corn Cob (Xylan) and Their Potential Application as Colon-Specific Drug Carrier. *Macromol. Symp.* **320**, 75–80 (2012).

88. Silva, A. E., Oliveira, E. E., Gomes, M. C. S., Marcelino, H. R., *et al.* Producing xylan/Eudragit® S100-based microparticles by chemical and physico-mechanical approaches as carriers for 5-aminosalicylic acid. *J. Microencapsul.* **30**, 787–795 (2013).

89. Malviya, T., Joshi, S., Dwivedi, L. M., Baranwal, K., *et al.* Synthesis of Aloevera/Acrylonitrile based Nanoparticles for targeted drug delivery of 5-Aminosalicylic acid. *Int. J. Biol. Macromol.* **106**, 930–939 (2018).

90. Hu, D., Liu, L., Chen, W., Li, S., *et al.* A Novel Preparation Method for 5-Aminosalicylic Acid Loaded Eudragit S100 Nanoparticles. *Int. J. Mol. Sci.* **13**, 6454–6468 (2012).

91. Pertuit, D., Moulari, B., Betz, T., Nadaradjane, A., *et al.* 5-amino salicylic acid bound nanoparticles for the therapy of inflammatory bowel disease. *J. Control. Release* **123**, 211–218 (2007).

92. Davoudi, Z., Peroutka-Bigus, N., Bellaire, B., Wannemuehler, M., *et al.* Intestinal Organoids Containing PLGA Nanoparticles for the Treatment of Inflammatory Bowel Diseases. *J. Biomed. Mater. Res. Part A* **106**, 876–886 (2018).

93. Banabid, W., Djerboua, F., Maiza, A., Bahri, Z. El, *et al.* Optimization and in-vitro Evaluation of Poly (lactic acid)/Mesalazine Microspheres as Drug Carriers. *Indian J. Pharm. Educ. Res.* **51**, s46–s53 (2017).

94. Moustafine, R. I., Viktorova, A. S. & Khutoryanskiy, V. V. Interpolymer complexes of carbopol ® 971 and poly(2-ethyl-2-oxazoline): Physicochemical studies of complexation and formulations for oral drug delivery. *Int. J. Pharm.* **558**, 53–62 (2019).

95. Gulbake, A. & Jain, S. K. Chitosan: a potential polymer for colon-specific drug delivery system. *Expert Opin. Drug Deliv.* **9**, 713–729 (2012).

96. Wouters, R. Inulin. in *Food Stabilisers, Thickeners and Gelling Agents* 180–197 (John Wiley & Sons, Ltd, 2009). doi:https://doi.org/10.1002/9781444314724.ch10.

97. Lemieux, M., Gosselin, P. & Mateescu, M. A. Carboxymethyl high amylose starch as excipient for controlled drug release: Mechanistic study and the influence of degree of substitution. *Int. J.*

Pharm. **382**, 172–182 (2009).

98. Kristensen, J. H. & Karsdal, M. A. Elastin. in *Biochemistry of Collagens, Laminins and Elastin* 197–201 (Elsevier Inc., 2016). doi:10.1016/B978-0-12-809847-9.00030-1.

99. Kielty, C. M., Sherratt, M. J. & Shuttleworth, C. A. Elastic fibres. *J. Cell Sci.* **115**, 2817 LP – 2828 (2002).

100. Raju, K. & Anwar, R. A. Primary Structures of Bovine Elastin a, b, and c Deduced from the Sequences of cDNA Clones. *J. Biol. Chem.* **262**, 5755–5762 (1987).

101. Cappello, J., Crissman, J., Dorman, M., Mikolajczak, M., *et al.* Genetic Engineering of Structural Protein Polymers. *Biotechnol. Adv.* **6**, 198–202 (1990).

102. Morelli, M. A. C., Debiasi, M., DeStradis, A. & M, T. A. An Aggregating Elastin-Like Pentapeptide. *J. Biomol. Struct. Dyn.* **11**, 181–190 (1993).

103. Simnick, A. J., Lim, D. W., Chow, D. & Chilkoti, A. Biomedical and Biotechnological Applications of Elastin-Like Polypeptides. *Polym. Rev.* **47**, 121–154 (2007).

104. Rodríguez-Cabello, J. C., Arias, F. J., Rodrigo, M. A. & Girotti, A. Elastin-like polypeptides in drug delivery. *Adv. Drug Deliv. Rev.* **97**, 85–100 (2016).

105. Rodríguez-Cabello, J. C., de Torre, I. G., Acosta, S., Salinas, S., *et al.* 4 - Elastin-like proteins: Molecular design for self-assembling. in *Woodhead Publishing Series in Biomaterials* (eds. Azevedo, H. S. & da Silva, R. M. P. B. T.-S. B.) 49–78 (Woodhead Publishing, 2018). doi:https://doi.org/10.1016/B978-0-08-102015-9.00004-6.

106. Quintanilla-Sierra, L., García-Arévalo, C. & Rodriguez-Cabello, J. C. Self-assembly in elastin-like recombinamers: a mechanism to mimic natural complexity. *Mater. Today Bio* **2**, (2019).

107. Girotti, A., Fernández-Colino, A., López, I. M., Rodríguez-Cabello, J. C., *et al.* Elastin-like recombinamers: Biosynthetic strategies and biotechnological applications. *Biotechnol. J.* **6**, 1174–1186 (2011).

108. Rodríguez-Cabello, J. C., Girotti, A., Ribeiro, A. & Arias, F. J. Synthesis of Genetically Engineered Protein Polymers (Recombinamers) as an Example of Advanced Self-Assembled Smart Materials. in *Nanotechnology in Regenerative Medicine: Methods and Protocols* (eds. Navarro, M. & Planell, J. A.) 17–38 (Humana Press, 2012). doi:10.1007/978-1-61779-388-2_2.

109. MacEwan, S. R. & Chilkoti, A. Applications of elastin-like polypeptides in drug delivery. *J. Control. Release* **190**, 314–330 (2014).

110. Nettles, D. L., Chilkoti, A. & Setton, L. A. Applications of elastin-like polypeptides in tissue engineering. *Adv. Drug Deliv. Rev.* **62**, 1479–1485 (2010).

111. Rodriguez-Cabello, J. C., Martín, L., Girotti, A., García-Arévalo, C., *et al.* Emerging applications of multifunctional elastin-like recombinamers. *Nanomedicine* **6**, 111–122 (2011).

112. Reguera, J., Lagarón, J. M., Alonso, M., Reboto, V., *et al.* Thermal Behavior and Kinetic Analysis of the Chain Unfolding and Refolding and of the Concomitant Nonpolar Solvation and Desolvation of Two Elastin-like Polymers. *Macromolecules* **36**, 8470–8476 (2003).

113. Machado, R., Ribeiro, A. J., Padrão, J., Silva, D., *et al.* Exploiting the sequence of naturally occurring elastin: Construction, production and characterization of a recombinant thermoplastic protein- based polymer. *J. Nano Res.* **6**, 133–145 (2009).

114. Bessa, P. C., Machado, R., Nürnberger, S., Dopler, D., *et al.* Thermoresponsive self-assembled elastin-based nanoparticles for delivery of BMPs. *J. Control. Release* **142**, 312–318 (2010).

115. Machado, R., da Costa, A., Pereira, A. M., Rodriguez-Cabello, J. C., *et al.* Elastins-Based Antimicrobial Particles for Delivery of Bioactive Compounds. in *Nanoparticles in Biology and Medicine: Methods and Protocols* (eds. Ferrari, E. & Soloviev, M.) 29–43 (Springer US, 2020). doi:10.1007/978-1-0716-0319-2_3.

116. Herrero-Vanrell, R., Rincón, A. C., Alonso, M., Reboto, V., *et al.* Self-assembled particles of an elastin-like polymer as vehicles for controlled drug release. *J. Control. Release* **102**, 113–122 (2005).

117. Costa, A., Pereira, A. M., Gomes, A. C., Rodriguez-Cabello, J. C., *et al.* Production of bioactive hepcidin by recombinant DNA tagging with an elastin-like recombinamer. *N. Biotechnol.* **46**, 45–53 (2018).

118. Machado, R., Azevedo-Silva, J., Correia, C., Collins, T., *et al.* High level expression and facile purification of recombinant silk-elastin-like polymers in auto induction shake flask cultures. *AMB Express* **3**, 1–15 (2013).

119. Schneider, C. A., Rasband, W. S. & Eliceiri, K. W. NIH Image to ImageJ: 25 years of image analysis.

Nat. Methods **9**, 671–675 (2012).

120. Zhang, Y., Huo, M., Zhou, J., Zou, A., *et al.* DDSolver: An Add-In Program for Modeling and Comparison of Drug Dissolution Profiles. *AAPS J.* **12**, 263–271 (2010).

121. da Costa, A., Machado, R., Ribeiro, A., Collins, T., *et al.* Development of Elastin-Like Recombinamer Films with Antimicrobial Activity. *Biomacromolecules* **16**, 625–635 (2015).

122. da Costa, A., Pereira, A. M., Gomes, A. C., Rodriguez-Cabello, J. C., *et al.* Single step fabrication of antimicrobial fibre mats from a bioengineered protein-based polymer. *Biomed. Mater.* **12**, 45011 (2017).

123. Trabbic-Carlson, K., Liu, L., Kim, B. & Chilkoti, A. Expression and purification of recombinant proteins from Escherichia coli: Comparison of an elastin-like polypeptide fusion with an oligohistidine fusion. *Protein Sci.* **13**, 3274–3284 (2004).

124. McPherson, D. T., Morrow, C., Minehan, D. S., Wu, J., *et al.* Production and purification of a recombinant elastomeric polypeptide, G-(VPGVG)19-VPGV, from Escherichia coli. *Biotechnol. Prog.* **8**, 347–352 (1992).

125. da Costa, A., Pereira, A. M., Sampaio, P., Rodríguez-Cabello, J. C., *et al.* Protein-Based Films Functionalized with a Truncated Antimicrobial Peptide Sequence Display Broad Antimicrobial Activity. *ACS Biomater. Sci. Eng.* (2021) doi:10.1021/acsbiomaterials.0c01262.

126. Reguera, J., Urry, D. W., Parker, T. M., McPherson, D. T., *et al.* Effect of NaCl on the Exothermic and Endothermic Components of the Inverse Temperature Transition of a Model Elastin-like Polymer. *Biomacromolecules* **8**, 354–358 (2007).

127. Pinedo-Martín, G., Santos, M., Testera, A. M., Alonso, M., *et al.* The effect of NaCl on the self-assembly of elastin-like block co-recombinamers: Tuning the size of micelles and vesicles. *Polymer (Guildf).* **55**, 5314–5321 (2014).

128. Valiaev, A., Lim, D. W., Schmidler, S., Clark, R. L., *et al.* Hydration and Conformational Mechanics of Single, End-Tethered Elastin-like Polypeptides. *J. Am. Chem. Soc.* **130**, 10939–10946 (2008).

129. Nelson, D. L. & Cox, M. M. Amino acids, Peptides and Proteins. in *Lehninger: Principles of Biochemistry* 78 (W. H. Freeman, 2004).

130. Widder, K., MacEwan, S. R., Garanger, E., Núñez, V., *et al.* Characterisation of hydration and

nanophase separation during the temperature response in hydrophobic/hydrophilic elastin-like polypeptide (ELP) diblock copolymers. *Soft Matter* **13**, 1816–1822 (2017).

131. Tan, J., Meng, N., Fan, Y., Su, Y., *et al.* Hydroxypropyl-β-cyclodextrin–graphene oxide conjugates: Carriers for anti-cancer drugs. *Mater. Sci. Eng. C* **61**, 681–687 (2016).

132. Siepmann, J. & Siepmann, F. Mathematical modeling of drug delivery. *Int. J. Pharm.* **364**, 328–343 (2008).

6. Annexes

Annex I

Protein nucleotide sequence and its characteristics

Sequence:

KKKVPAVGVPAVGVPAVGVPAVGVPAVGVPAVGVPAVGVPAVGVPAVGVPAVGVPAVGVPAVGVPA
VGVPAVGVPAVGVPAVGVPAVGVPAVGVPAVGVPAVGVPAVGVPAVGVPAVGVPAVGVPAVGVPAV
GVPAVGVPAVGVPAVGVPAVGVPAVGVPAVGVPAVGVPAVGVPAVGVPAVGVPAVGVPAVGVPAVG
VPAVGVPAVGVPAVGVPAVGVPAVGVPAVGVPAVGVPAVGVPAVGVPAVGVPAVGVPAVGVPAVGV
PAVGVPAVGVPAVGVPAVGVPAVGVPAVGVPAVGVPAVGVPAVGVPAVGVPAVGVPAVGVPAVGVP
AVGVPAVGVPAVGVPAVGVPAVGVPAVGVPAVGVPAVGVPAVGVPAVGVPAVGVPAVGVPAVGVPAV
GVPAVGVPAVGVPAVGVPAVGVPAVGVPAVGVPAVGVPAVGVPAVGVPAVGVPAVGVPAVGVPAVG
VPAVGVPAVGVPAVGVPAVGVPAVGVPAVGVPAVGVPAVGVPAVGVPAVGVPAVGVPAVGVPAVGV
PAVGVPAVGVPAVGVPAVGVPAVGVPAVGVPAVGVPAVGVPAVGVPAVGVPAVGVPAVGVPAVGVP
AVGVPAVGVPAVGKKK

Molecular weight: 85.49 kDa

Theoretical isoelectric point: 10.70

Annex II

Polyacrylamide 10 % gels used in SDS-PAGE

Reagents/solutions	Volume
Running buffer	
Acrylamide/bisacrylamide (40:2) solution	1.4 mL
0.75 M Tris-HCl, 0.2 % SDS, pH 8.8 buffer	2.8 mL
dH2O	1.35 mL
APS 10 %	30 µL
TEMED	3.5 µL
Stacking buffer	
Acrylamide/bisacrylamide (40:2) solution	0.28 mL
0.25 M Tris-HCl, 0.2 % SDS, pH 6.8 buffer	1.1 mL
dH2O	0.9 mL
APS 10 %	12.5 µL
TEMED	4 µL

Loading buffer 5 X used for SDS-PAGE samples

SDS 10 %
Glycerol 40 %
Tris-HCl 0.2 M
β-mercaptoethanol 50 mM
Bromophenol Blue 0.1 %

Annex III

Absorbance spectrum of 5-ASA

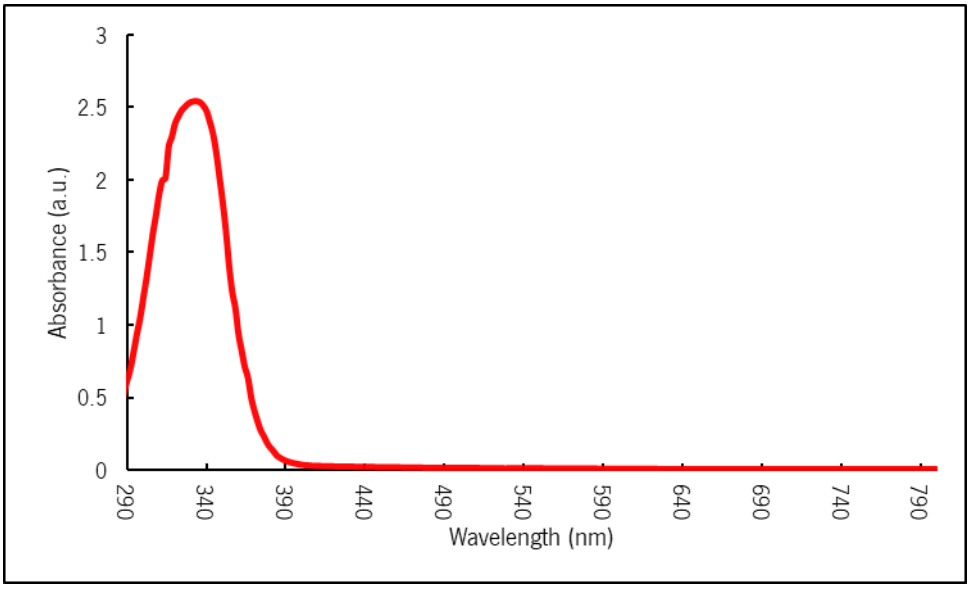

Fluorescence spectrum of 5-ASA